



# PDK1 regulates auxin transport and *Arabidopsis* vascular development through AGC1 kinase PAX

Yao Xiao <sup>1,2</sup> and Remko Offringa <sup>1</sup> ✉

**The 3-phosphoinositide-dependent protein kinase 1 (PDK1) is a conserved master regulator of AGC kinases in eukaryotic organisms. *pdk1* loss of function causes a lethal phenotype in animals and yeasts, but only mild phenotypic defects in *Arabidopsis thaliana* (*Arabidopsis*). The *Arabidopsis* genome contains two PDK1-encoding genes, *PDK1* and *PDK2*. Here, we used clustered regularly interspaced short palindromic repeat (CRISPR)/CRISPR-associated protein 9 (Cas9) to generate true loss-of-function *pdk1* alleles, which, when combined with *pdk2* alleles, showed severe developmental defects including fused cotyledons, a short primary root, dwarf stature and defects in male fertility. We obtained evidence that PDK1 is responsible for AGC1 kinase PROTEIN KINASE ASSOCIATED WITH BRX (PAX) activation by phosphorylation during vascular development, and that the PDK1 phospholipid-binding Pleckstrin Homology domain is not required for this process. Our data indicate that PDK1 regulates polar auxin transport by activating AGC1 clade kinases, resulting in PIN phosphorylation.**

PDK1 is a conserved protein serine/threonine kinase in eukaryotes. It is well known for its key role as activator of other AGC kinases that play crucial roles in basal cellular functions in lower (yeast) and higher (human/mouse) eukaryotes. PDK1 typically contains a kinase domain at its N terminus with a PDK1-interacting fragment (PIF)-binding pocket for AGC kinase interaction, and a pleckstrin homology (PH) domain at the C terminus for PDK1 plasma membrane (PM) recruitment and kinase activity regulation<sup>1–4</sup>. *Physcomitrella patens* PDK1 (PpPDK1) and the yeast PDK1 orthologues (ScPKH1 and ScPKH2) lack a PH domain but are still functional<sup>5–8</sup>, indicating that the PH domain is not required in all eukaryotes<sup>9</sup>. Complete loss of function of *PDK1* is lethal for yeasts, fruit flies and mice<sup>5,6,10,11</sup>. In plants, although several genetic approaches have been employed in different species to analyse PDK1 function, the results obtained to date do not yet give a clear picture<sup>8,12,13</sup>. *Arabidopsis thaliana* (*Arabidopsis*) has two highly homologous *PDK1* genes, At5g04510 (*AtPDK1.1*) and At3g10540 (*AtPDK1.2*), which we renamed *PDK1* and *PDK2*, respectively. Double mutants containing the currently available *pdk1* and *pdk2* transfer DNA (T-DNA) insertion alleles show only a weak developmental defect with reduced silique length and plant height<sup>14,15</sup>. In contrast, loss-of-function mutants in *Arabidopsis* genes encoding AGC kinases phosphorylated by PDK1 in vitro, including the AGC3 kinase PINOID (PID) and the AGC1 kinases OXIDATIVE SIGNAL INDUCIBLE 1 (OXI1), UNICORN (UCN) and most other AGC1 clade members<sup>15–19</sup>, show strong defects, indicating that they play important roles in plant development or defence<sup>12,15,18,20–27</sup>. AGC1 kinase PROTEIN KINASE ASSOCIATED WITH BRX (PAX/AGC1.3) is one of these in vitro substrates of PDK1<sup>17,18</sup>. Loss-of-function mutations in *PAX* lead to a shorter primary root caused by protophloem differentiation defects. PAX phosphorylates PIN-FORMED (PIN) auxin efflux carriers and operates, together with its auxin-sensing repressor BREVIS RADIX (BRX), as a molecular rheostat in regulating auxin transport activity during root protophloem differentiation. PAX requires activation by phosphorylation at S596, but the activating kinase has not yet been identified<sup>28</sup>.

Here we show that the published *pdk1* T-DNA insertion alleles do not lead to loss of function, explaining the lack of strong phenotypes in previously published *pdk1 pdk2* double mutants<sup>14,15</sup>. Using clustered regularly interspaced short palindromic repeat (CRISPR)/CRISPR-associated protein 9 (Cas9), we generated several true *pdk1* loss-of-function mutant alleles which, when combined with the *pdk2* T-DNA insertion allele, displayed strong growth and developmental defects. The mutant phenotypes and complementation experiments indicate a PID-independent role for PDK1 in plant development as activator of PAX and, most probably, other AGC1 clade kinases, fine-tuning auxin transport during vascular differentiation, male gametophyte development and differential growth responses.

## Results

**CRISPR/Cas9-generated mutant alleles indicate a central role for PDK1 in development.** In view of the model previously proposed that PDK1 regulates PID kinase activity<sup>16</sup>, we expected *PDK1* overexpression (*PDK1ox*) to cause similar phenotypes as *PID* overexpression (*PIDox*) in *Arabidopsis*. These are agravitropic seedling growth and collapse of the main root meristems as a result of redirected polarity of PIN-mediated auxin transport (Extended Data Fig. 1g,h,j)<sup>21,29</sup>. Surprisingly, however, all of the representative *PDK1ox* lines, generated with *p35S::YFP:PDK1* or *p35S::PDK1* constructs, showed normal gravitropic seedling growth and no collapse of the main root meristem was observed (Extended Data Fig. 1a–j). Mature *PDK1ox* plants developed and flowered like wild-type *Arabidopsis* plants (Extended Data Fig. 1k,l). The above results suggested that elevated PDK1 levels do not lead to increased PID activity.

Next we reassessed the previously described *pdk* loss-of-function mutant alleles<sup>14,15</sup>. Two *pdk2* alleles, *pdk2-1* and *pdk2-4* (Supplementary Fig. 1a), were confirmed to be true knockout mutants by PCR with reverse transcription (RT-PCR) analysis (Fig. 1a). However, in contrast to published data, the *pdk1-c* allele<sup>15</sup> appeared to produce a full-length messenger RNA (Fig. 1a) whereas the *pdk1-a* and *pdk1-b* alleles<sup>14,15</sup> produced a partial or mutated

<sup>1</sup>Plant Developmental Genetics, Institute of Biology Leiden, Leiden University, Leiden, the Netherlands. <sup>2</sup>Present address: Plant Systems Biology, TUM School of Life Sciences Weihenstephan, Technical University of Munich, Freising, Germany. ✉e-mail: [r.offringa@biology.leidenuniv.nl](mailto:r.offringa@biology.leidenuniv.nl)

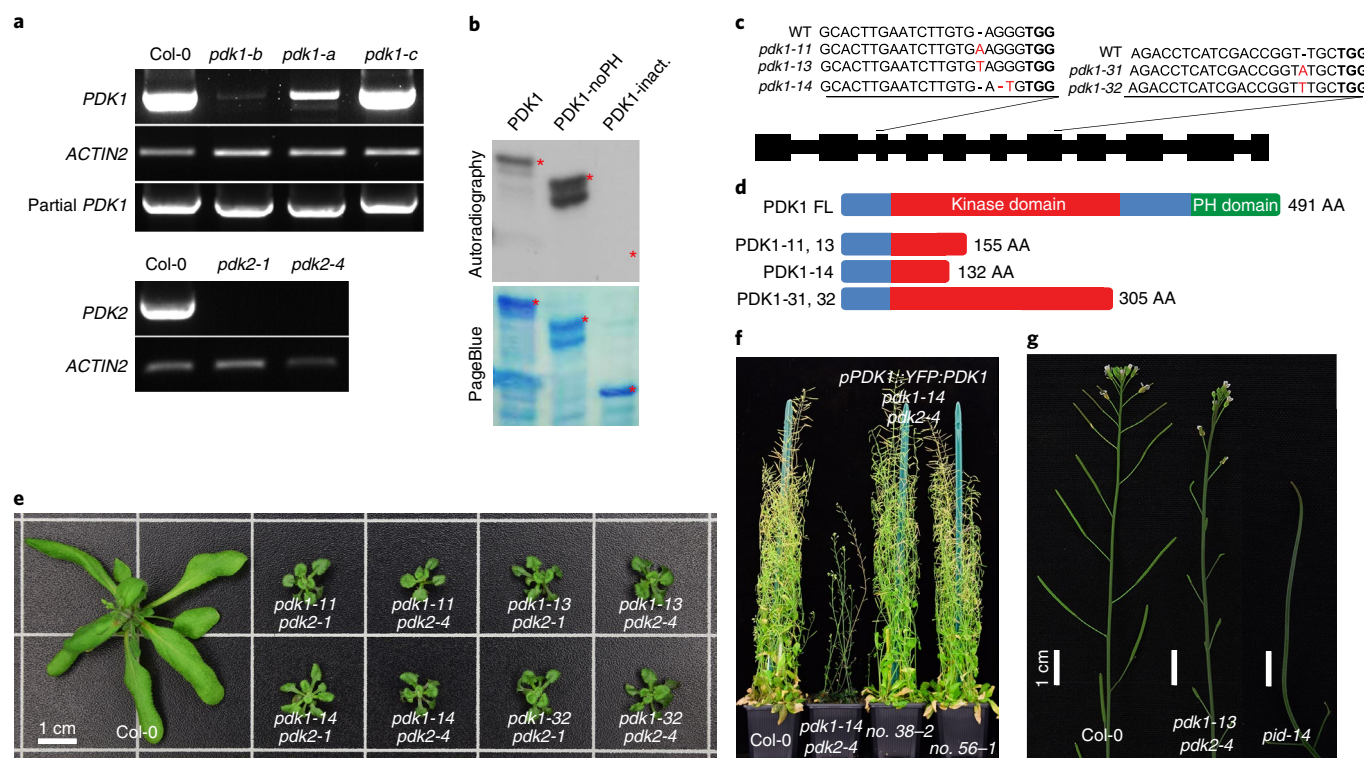


**Fig. 1 | Arabidopsis *pdk1 pdk2* loss-of-function mutants exhibit a dwarf stature, but do not phenocopy *pid* mutants.** **a**, Semi-quantitative RT-PCR was used to detect *PDK1* or *PDK2* expression in the different *Arabidopsis pdk1* or *pdk2* T-DNA insertion mutant alleles, respectively. **b**, Autophosphorylation activity of purified glutathione-S-transferase (GST)-*PDK1* and GST-*PDK1*-noPH (lacking PH domain, size similar to that of partial *PDK1* in *pdk1-b*). A GST-tagged inactive *PDK1* version with only half of the kinase domain (amino acids 1–213) was used as negative control (*PDK1*-inact.). GST-tagged protein bands are indicated by red asterisks. **c**, Schematic representation of part of the *PDK1* gene with the gRNA target sites and resulting mutations in the newly obtained CRISPR/Cas9-generated alleles. The protospacer adjacent motif (PAM) sequence for Cas9 is highlighted in bold; inserted or replaced nucleotides in the new mutant alleles are highlighted in red. Mutant alleles obtained at editing site 1 (third exon) and site 3 (seventh exon) are named *pdk1-1n* and *pdk1-3n*, respectively. Since *pdk1-12* and *pdk1-13* have the same ‘T’ insertion, only the latter is shown. WT, wild type; AA, amino acids. **d**, Schematic linear representation of the full-length (FL, 491 amino acids) *PDK1* protein (protein kinase domain: amino acids 44–311; PH domain: amino acids 386–491; <https://www.uniprot.org>) and the shorter versions produced in alleles *pdk1-11*, -13, -14, -31 and -32. **e**, Rosette phenotype of 30-day-old wild-type *Arabidopsis* (Col-0) and eight different *pdk1 pdk2* loss-of-function allelic combinations. **f**, Introduction of *pPDK1::YFP:PDK1* into the *pdk1-14 pdk2-4* background completely rescued the mutant phenotype. **g**, Inflorescence phenotype of wild-type *Arabidopsis* (Col-0) and mutants *pdk1-3 pdk2-4* and *pid-14*. **a, b**, Similar results were obtained in three independent experiments. **e, g**, Similar phenotypes were observed in four independent experiments.

mRNA (Fig. 1a and Supplementary Fig. 1), leading to the expression of a *PDK1* protein lacking its PH domain (Supplementary Fig. 1) but showing high autophosphorylation activity (Fig. 1b). Based on these findings, we concluded that the three published *pdk1* T-DNA insertion alleles are not likely to be true loss-of-function mutants.

To obtain true *pdk1* loss-of-function mutants, we designed guide RNAs against the third and seventh exons and were able to obtain five CRISPR/Cas9-induced mutants with frame shifts in the *PDK1* open-reading frame (Fig. 1c,d). Like the *pdk1* T-DNA insertion alleles, these new *pdk1* mutant alleles did not show major morphological differences from the wild type. However, when combined with the *pdk2-1* or *pdk2-4* allele, all double-mutant combinations showed the same marked dwarf phenotype (Fig. 1e–g and Extended Data Fig. 2a–c). Complementation analysis using either *p35S::PDK1*, *p35S::YFP:PDK1* or *pPDK1::YFP:PDK1* showed that the dwarf phenotype was caused by *pdk* loss of function (Fig. 1f and Extended Data Fig. 2d–k). These results suggest that *PDK1* and *PDK2* act redundantly and have a considerably more important role in plant growth and development than was previously reported. *pdk* loss of function leads to many developmental defects, but not to a *pid* phenocopy.

Besides the decreased rosette diameter and reduced final plant height (Fig. 1e,f and Extended Data Fig. 2a), *pdk1 pdk2* double-mutant plants flowered much later and showed strong reproductive defects (Extended Data Figs. 2b,c and 3). The frequency of double-homozygous F2 progeny was much lower (1 in  $47.7 \pm 2.6$ ) than the expected Mendelian ratio (1 in 16). In addition, F2 plants with the *pdk1(-/-) pdk2(±)* or *pdk1(±) pdk2(-/-)* genotype produced homozygous progeny at a much lower frequency than the expected 1:4 ratio (Supplementary Table 1). Seed production of the homozygous *pdk1 pdk2* mutants ( $1.5 \pm 0.21$  per silique for *pdk1-13 pdk2-4*) was significantly reduced compared to the wild type ( $65.9 \pm 0.61$  per silique) and, as a result, mutant plants developed short siliques (Extended Data Fig. 3a). These results implied that *pdk1 pdk2* loss of function caused gametophyte and/or embryo development defects in *Arabidopsis*. Reciprocal crosses between wild-type and *pdk1-13 pdk2-4* double-mutant plants revealed that, in particular, male gametophyte development was strongly impaired by *pdk1* loss of function (Extended Data Fig. 3j). Alexander staining showed that pollen grain development in the *pdk1 pdk2* double mutant was not aborted, but that anther dehiscence was the major cause of male fertility problems (Extended Data Fig. 3b–e,i). In addition, in vitro germinated *pdk1 pdk2* pollen produced much

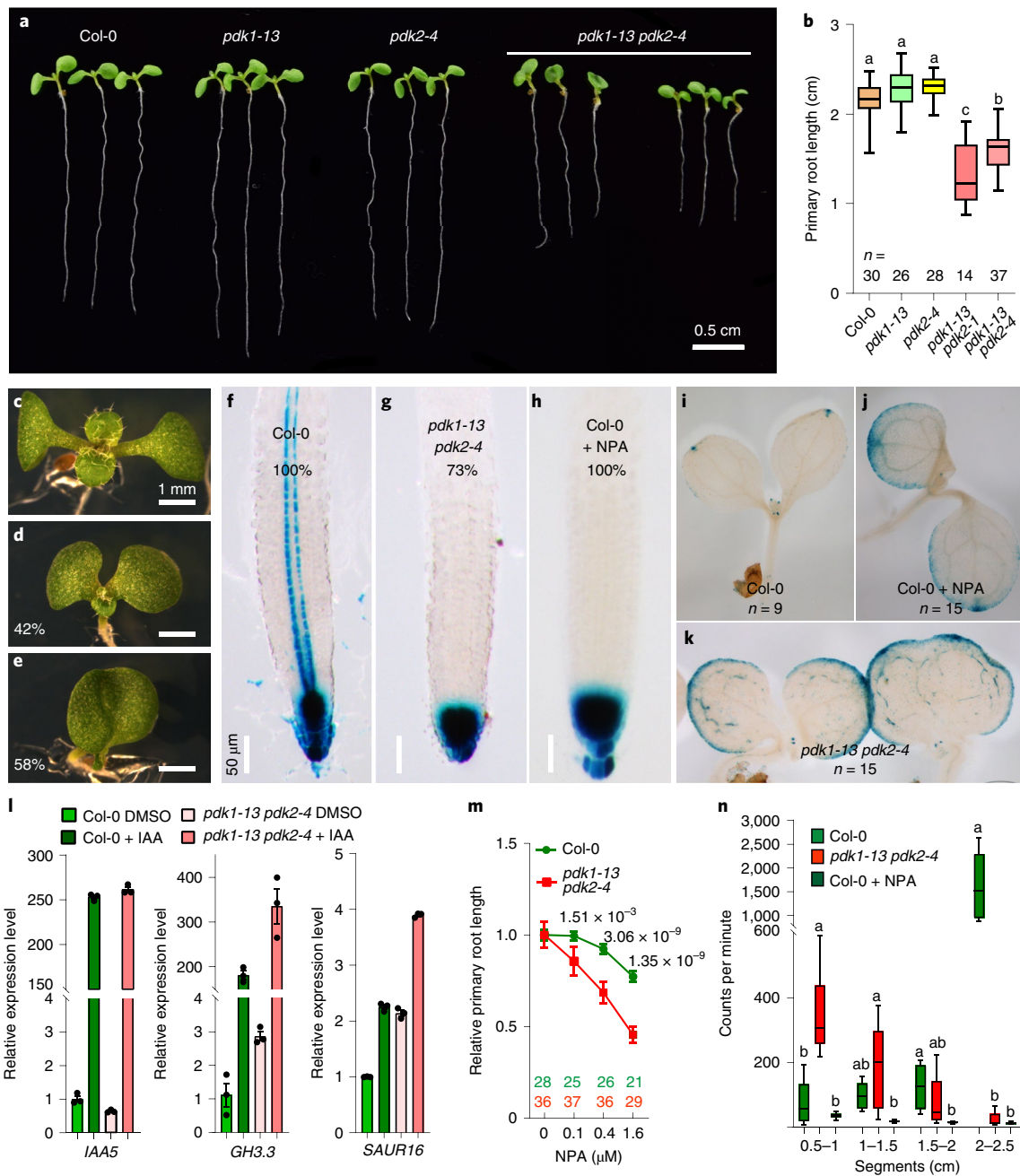


**Fig. 2 | The phenotype and auxin response pattern of *pdk1 pdk2* mutant seedlings resembles that of auxin transport inhibitor-treated seedlings.**

**a**, The phenotype of 7-day-old wild-type (Col-0) and *pdk1 pdk2* mutant seedlings. Similar results were obtained in six independent experiments. **b**, Primary root length of 7-day-old seedlings. Lower case letters (a, b, c) indicate averages that are significantly different, as tested by one-way analysis of variance (ANOVA) followed by Tukey's test ( $P < 0.05$ ; details of statistical analysis are provided in Supplementary Table 4);  $n$  indicates the number of independent plants. **c–e**, Cotyledon phenotype of wild-type (Col-0) seedlings (**c**,  $n = 84$  independent seedlings), showing two symmetrically distributed cotyledons with extended petioles, or *pdk1-13 pdk2-4* seedlings, of which 42% are positioned at an angle with short petioles (**d**) and 58% show fused cotyledons (**e**,  $n = 460$  independent seedlings). **f–k**, Histochemical GUS staining of 7-day-old wild-type seedlings (Col-0, **f,i**), wild-type seedlings grown on  $0.5 \mu\text{M}$  NPA (Col-0 + NPA, **h,j**) or *pdk1-13 pdk2-4* seedlings (**g,k**), all three groups containing the *pDR5::GUS* auxin response reporter. **f–h**, Percentages indicate the ratio of representative image of the observed seedlings ( $n = 15$ ). The remaining 27% of *pdk1-13 pdk2-4* shows strongly decreased, but not absent, *pDR5::GUS* signal in the stele. **b–k**, Similar results were obtained in three independent experiments. **l**, RT-qPCR analysis of auxin-induced expression of *IAA5*, *GH3.3* and *SAUR16* in 5-day-old *Arabidopsis* wild-type (Col-0) and *pdk1-13 pdk2-4* mutant seedlings. Bars indicate the mean, and the error bars s.e.m. ( $n = 3$  technical repeats). Three independent experiments yielded similar results. **m**, NPA sensitivity of wild-type (Col-0) and *pdk1-13 pdk2-4* based on the primary root length of seedlings grown on medium with increasing NPA concentration. A two-sided Student's  $t$ -test was used for analysis between Col-0 and *pdk1-13 pdk2-4* from the same NPA concentration,  $P$  values are shown above each comparison. Green dots or red squares indicate the mean, and error bars the 95% confidence intervals. Green and red numerals indicate the numbers of independent seedlings used. **n**, Transport of  $^3\text{H}$ -IAA in 2.5-cm wild-type (Col-0), wild-type with NPA and *pdk1-13 pdk2-4* inflorescence stem pieces ( $n = 8$  independent stem pieces). Data were analysed using one-way ANOVA followed by Tukey's test. Significant differences are indicated by different lower case letters in each segment group ( $P < 0.05$ ; details of statistical analysis are provided in Supplementary Table 4). **m, n**, Representative experiments of four biological repeats displaying similar results are shown. **b, n**, Boxes indicate first and third quartile, horizontal lines in boxes the median, and whiskers the maximum and minimum.

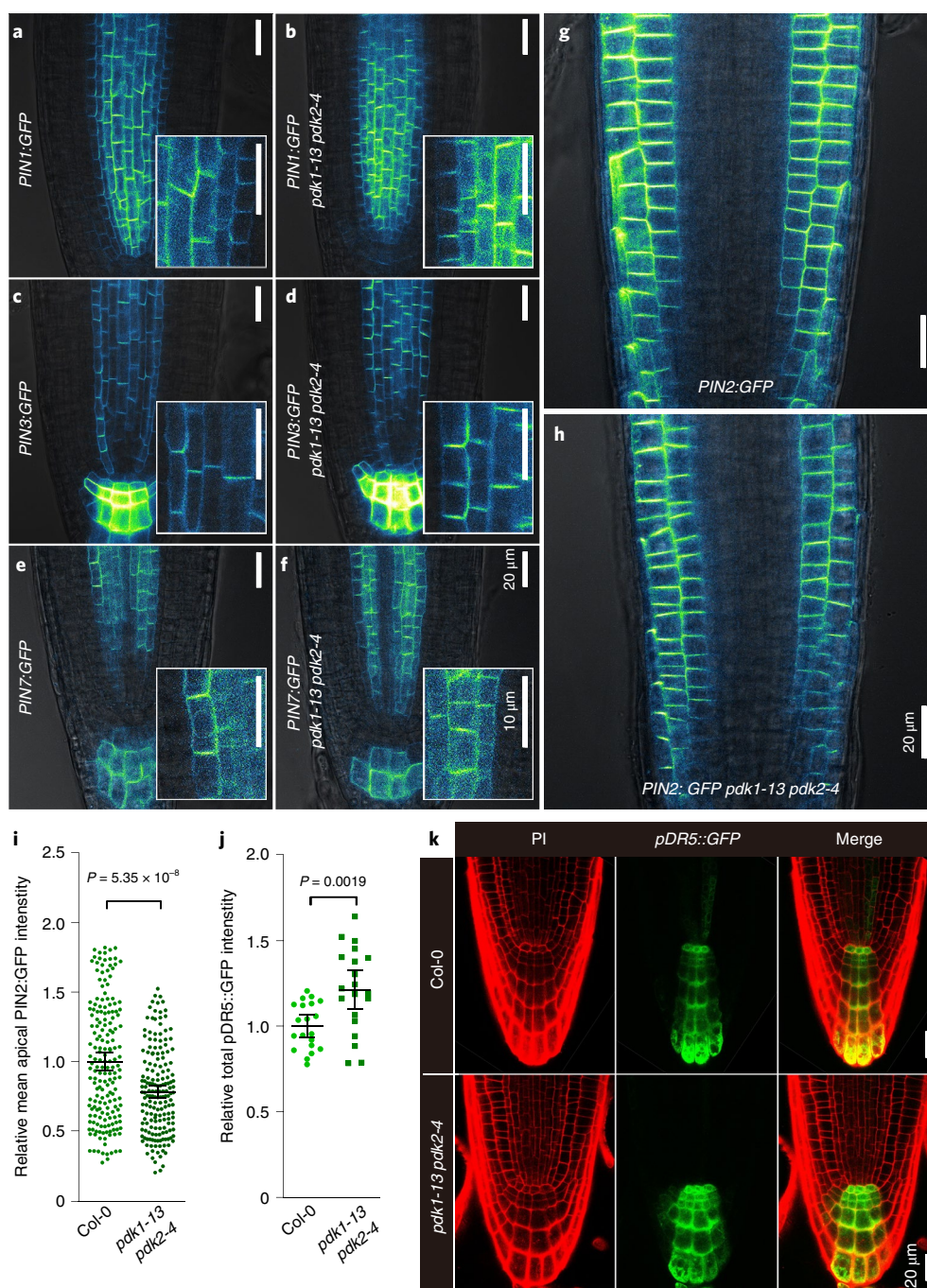


**Fig. 3 | PDK1 is not involved in PIN polarity control.** **a–h**, Confocal images showing the subcellular localization of PIN1:GFP (**a,b**), PIN3:GFP (**c,d**), PIN7:GFP (**e,f**) and PIN2:GFP (**g,h**) in wild-type (Col-0, **a,c,e,g**) or *pdk1-13 pdk2-4* mutant (**b,d,f,h**) root tips. Insets in **a–f** show the details of PIN polarity in stele cells. Four biological repeats showed similar results, and 12 independent roots were observed in each experiment. **i,j**, Relative total GFP intensity of PIN2:GFP at the apical side of epidermal cells ( $n = 181$  or 177 cells from eight independent wild-type (Col-0) or *pdk1-13 pdk2-4* mutant roots, **i**) and by *pDR5::GFP* expression in columella-quiescent centre cells ( $n = 20$  independent wild-type (Col-0) or *pdk1-13 pdk2-4* mutant roots, **j**). PIN2:GFP and *pDR5::GFP* intensities are shown relative to the Col-0 control. Four biological repeats showed similar results. Means with 95% confidence intervals are indicated. A two-sided Student's *t*-test was used for statistical analysis. **k**, Confocal images of *pDR5::GFP* expression in a wild-type (Col-0) and a *pdk1-13 pdk2-4* mutant root tip. Left: PI staining; middle: GFP signal; right: merged image. Representative images are from one of three independent experiments. Twenty wild-type or *pdk1-13 pdk2-4* mutant roots were observed in each experiment.

shorter and aberrantly shaped pollen tubes as a result of defective tip growth (Extended Data Fig. 3f–h), which resembles the *agc1.5 agc1.7* mutant phenotype<sup>26</sup>. This is in line with the finding that PDK1 was identified in a yeast two-hybrid screen using AGC1.5 as the bait<sup>27</sup>, and that it phosphorylates AGC1.5 and AGC1.7 *in vitro*<sup>17</sup>.

The ovules of double-mutant plants did not show noticeable morphological alterations (Extended Data Fig. 3k,l), which is in line with a predominant effect of *pdk* loss of function on male fertility.

In contrast to fertility problems, *pdk1 pdk2* double mutants developed relatively normal flowers showing no clear patterning defects.

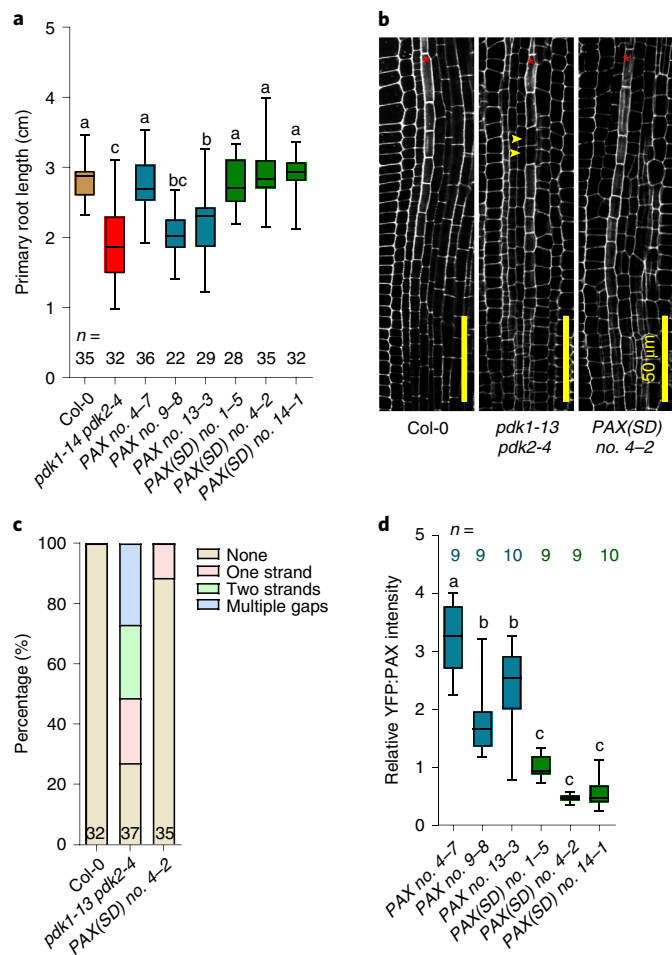


**Fig. 4 | PDK1-dependent activation of PAX directs protophloem differentiation.** **a–c**, Primary root length of 8-day-old (**a**) and PPSE defects in 5-day-old (**b,c**) wild-type, *pdk1 pdk2*, *pdk1 pdk2 pPDK1::YFP:PAX* (*PAX*) and *pdk1 pdk2 pPDK1::YFP:PAX(SD)* (*PAX(SD)*) seedlings. **a**, The number of seedlings measured (*n*) is indicated for each line. **b**, The protophloem cell layers are marked with red asterisks, and yellow arrowheads indicate gap locations. **c**, Numbers in columns represent the number of independent roots observed. **d**, Relative *PAX* expression level in the indicated lines, as determined by YFP:*PAX* fluorescence intensity in columella cells. Numbers above the box plot (*n*) indicate the number of independent roots observed. The average intensity in line *YFP:PAX(SD)* no. 1–5 was set at 1. **a,d**, Statistically different groups are indicated by lower case letters, as determined by one-way ANOVA followed by Tukey's test ( $P < 0.05$ ; details of statistical analysis are provided in Supplementary Table 4). Boxes indicate the first and third quartile, the horizontal line in a box the median, and whiskers the maximum and minimum. Similar results were obtained in three independent experiments.

Flowers did show early stigma exposure due to impaired sepal growth, and slightly reduced filament elongation (Extended Data Fig. 3i). The lack of phenotypic resemblance between *pdk1-13 pdk2-4* and *pid-14* inflorescences and flowers (Fig. 1g) suggested that PDK1 is not essential for full PID function during inflorescence development. Moreover, expression of a PID:YFP fusion in *pdk1-13 pdk2-4* protoplasts showed that PDK1 activity is not necessary for the predominant localization of PID at the PM (Extended Data Fig. 1m). Based on these results and the overexpression data we concluded, in contrast to what has previously been hypothesized<sup>16,17</sup>, that PDK1 is not a key regulator of PID activity.

**Auxin transport is impaired in *pdk1 pdk2* mutants.** Even though *PDK1* overexpression and loss-of-function phenotypes did not point to an important role for PDK1 in PID function, the *pdk1-13 pdk2-4* mutant seedling phenotypes did suggest involvement of PDK1 in the regulation of auxin response or transport (Fig. 2a–e). Mutant primary roots showed normal growth up to 2 d after germination, following which their growth rate declined (Fig. 2a,b) and roots started to oscillate randomly with a large amplitude, resulting in curved, short roots (Extended Data Fig. 4a). The cotyledons of *pdk1-13 pdk2-4* seedlings were either fused (58%) or positioned at an abnormal angle ( $<180^\circ$ , 42%) (Fig. 2c–e). Expression of the *pDR5::GUS* auxin response reporter was absent or strongly decreased in the root stele of *pdk1-13 pdk2-4* mutant seedlings and confined to the root tip, while expression was enhanced in both mutant cotyledon margins and fragmented cotyledon veins (Fig. 2f,g,i,k). This closely resembled the *pDR5::GUS* expression of 7-day-old seedlings grown on medium supplemented with the auxin transport inhibitor naphthylphthalamic acid (NPA) (Fig. 2h,j)<sup>30,31</sup>. Moreover, the increase in *pDR5::GUS* expression in cotyledons corroborated that *pdk1-13 pdk2-4* mutants are defective in auxin transport, rather than in auxin biosynthesis or signalling. Short-term treatment of wild-type and *pdk1-13 pdk2-4* seedlings with indole-3-acetic acid (IAA) and subsequent quantitative PCR with reverse transcription (RT-qPCR) analysis showed that auxin-inducible expression of genes *IAA5*, *GH3.3* and *SAUR16* was not impaired, confirming that the mutants are not defective in auxin response (Fig. 2l). Instead, *pdk1-13 pdk2-4* mutant seedlings were hypersensitive to NPA treatment compared to the wild type (Fig. 2m). Moreover, the auxin transport capability of *pdk1-13 pdk2-4* inflorescence stems was significantly reduced compared to that of wild-type stems (Fig. 2n). Together, the above data pointed toward a role for PDK1 in enhancing polar auxin transport.

Based on promoter–reporter and complementing gene–reporter fusions, *PDK1* appeared to be strongly expressed in (pro)vascular tissues from the early globular embryo stage, and in the columella root cap (Extended Data Fig. 5a–k). The gene also showed more general expression in young hypocotyls, cotyledons, leaves and floral organs, and in growing siliques (Extended Data Fig. 5l–n,r,s). The expression pattern observed for *pPDK2* was highly comparable to that of *PDK1* (Extended Data Fig. 5o–q,t,u), except that expression was observed in neither the root apex (Extended Data Fig. 5p) nor embryos (data not shown). The expression in (pro)vascular tissues corroborated the proposed function for PDK1 as a regulator of auxin transport.

**PDK1 is not likely to regulate auxin efflux by direct PIN phosphorylation.** PDK1 is polarly localized at the basal (rootward) side of root stele cells (Extended Data Fig. 5k), where it co-localizes with PIN1, PIN3 and PIN7 (Fig. 3a,c,e). This observation prompted us to test whether PIN proteins are directly phosphorylated by PDK1. In vitro phosphorylation assays showed that only the PIN2 central hydrophilic loop (PIN2HL) and the PIN2HL S1,2,3A version, in which the three target serines for PID are substituted by alanines, are highly phosphorylated by PDK1, whereas the PIN1-, PIN3- and PIN7HL are only very weakly phosphorylated (Extended Data Fig. 6). Based on published in vitro phosphorylation data, we deduced that PDK1 preferentially phosphorylates the second serine residue in the conserved RSXS<sub>F</sub>VG motif (X represents any amino acid) located in the activation segment of AGC kinases<sup>16,17</sup>. Analysis of the PIN2HL identified five RXXS motifs in the PIN2HL (RVDS<sup>179</sup>, RRSS<sup>210</sup>, RASS<sup>259</sup>, RMS<sup>331</sup> and RGSS<sup>409</sup>), and the strong in vitro phosphorylation signal suggests that several of these motifs are PDK1 targets. However, PIN2 did not show co-expression with PDK1 (Extended Data Fig. 5k and Fig. 3g), indicating that this has no relevance in vivo. In the three other PIN proteins showing co-expression in the root stele or columella cells, one RXXS motif was identified in the PIN1HL (RGSS<sup>253</sup>) and one in

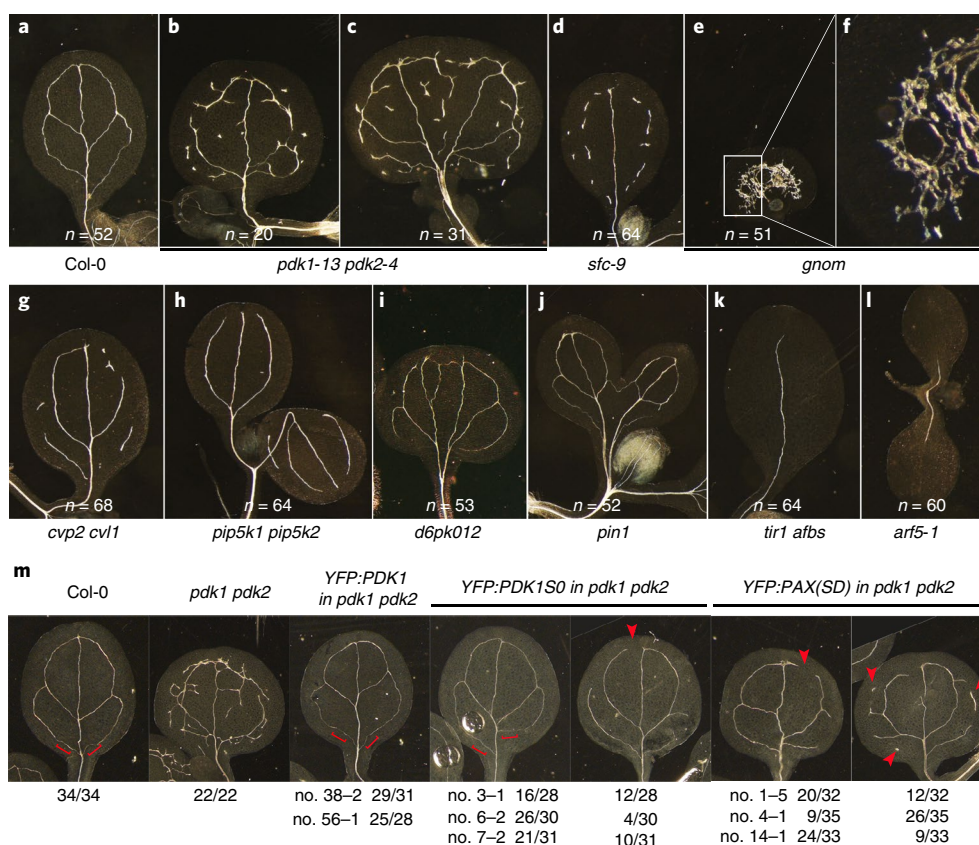


**Fig. 5 | The unique *pdk1-13 pdk2-4* mutant cotyledon vein pattern can be partially rescued by PDK1S0 and PAX(SD).** **a–l**, Dark-field images showing the vein pattern in cleared cotyledons of 7-day-old seedlings of wild-type *Arabidopsis* (*Col-0*), a *pdk1 pdk2* double mutant and several other indicated single, double or triple mutants. The comparison shows that *pdk1 pdk2* mutant cotyledons have a unique vein pattern. For each line, a representative image was selected from the indicated number (*n*) of observed cotyledons. **i**, *d6pk012* denotes *d6pk d6pk11 d6pk12*. **k**, *tir1 afbs* denotes *tir1-1 afb1-3 afb2-3 afb3-4*. **m**, *pPDK1::YFP:PDK1S0* and *pPDK1::YFP:PAX(SD)* partially rescued cotyledon vein breaks in *pdk1 pdk2*. The fraction of the total number of observed cotyledons showing a similar phenotype is indicated below each image. Cotyledons showing vein pattern breaks at positions indicated with red brackets are classified in the same group as those with continuous veins. Red arrowheads denote break locations and isolated islands. **a–m**, Similar results were obtained in three independent experiments.

the PIN7HL (RCNS<sup>431</sup>), but no motif was found in the PIN3HL. No noticeable alteration in polarity or abundance was observed for PIN1, PIN3 and PIN7 in *pdk1-13 pdk2-4* mutant roots (Fig. 3a–f). Whether the observed weak in vitro PIN phosphorylation by PDK1 is relevant for the in vivo function of these three PIN proteins remains to be established. The abundance of PIN2:green fluorescent protein (GFP) was slightly decreased in *pdk1-13 pdk2-4* mutant root tips (Fig. 3g–i), but this might be an indirect effect of *pdk* loss of function on auxin distribution in the root tip because we measured a slight increase in *pDR5::GFP* signal in *pdk1-13 pdk2-4* mutant versus wild-type root tips (Fig. 3j,k).

**PDK1 is part of the auxin-sensing rheostat regulating proto-phloem differentiation.** Several in vitro PDK1 phosphorylation substrates are AGC1 kinases that have been reported to regulate auxin transport by direct phosphorylation of PIN auxin efflux carriers<sup>17,28,32,33</sup>. The fact that their loss-of-function mutants share phenotypic defects with the *pdk1-13 pdk2-4* mutant, such as the short root of the *pax* mutant<sup>28</sup> (Fig. 2a), or disturbed hypocotyl tropic growth and lateral root development of the *d6pk012* (*d6pk d6pk11 d6pk12*) triple mutant<sup>24</sup> (Extended Data Fig. 4), hinted that PDK1 might regulate auxin transport by phosphorylating and activating these AGC1 clade kinases.

*PDK1* and *PDK2* both showed expression in the root stele, where PDK1 co-localized with PIN proteins and PAX at the basal PM of

proto-phloem cells (Fig. 3a,c,e and Extended Data Figs. 5k and 7a,b)<sup>28</sup>. As in the *pax* mutant, the short root phenotype of *pdk1 pdk2* mutants coincided with defects in proto-phloem differentiation, leading to a high frequency of gaps in proto-phloem sieve elements (PPSEs) (Extended Data Fig. 7c–e). Phosphorylation of PAX at S<sup>596</sup>, which is a PDK1 in vitro target<sup>17,18</sup>, has been reported to be induced by auxin to fine-tune auxin concentration during proto-phloem differentiation<sup>17,18,28</sup>. Introduction of a construct with the *PDK1* promoter driving expression of the phosphomimetic YFP–PAX(S596D) fusion (PAX(SD)) in the *pdk1 pdk2* mutant background completely restored proto-phloem differentiation and primary root growth (Fig. 4a–c). Gravitropic growth was also partially restored in PAX(SD) *pdk1 pdk2* roots (Extended Data Fig. 8m–o). *PDK1* promoter-driven expression of a wild-type YFP–PAX fusion (PAX) rescued primary root growth only when the fusion gene was expressed at a higher level (Fig. 4a,d and Extended Data Fig. 8j–l). In comparison, for the *PDK1::YFP:PAX(SD)* construct we obtained lines with only a low expression level but this was sufficient for complementation (Fig. 4d). These results indicated that PDK1 is among the PAX-activating kinases in the rheostat that controls auxin transport during proto-phloem differentiation. The complementation of *pdk1 pdk2* by wild-type PAX suggested that PAX is sufficiently active when expressed at higher levels. The fact that we did not obtain higher-expressing lines for the *PDK1::YFP:PAX(SD)* construct corroborates the previous observation that PAX(SD) over-expression has detrimental effects on root development<sup>26</sup>. PAX(SD)

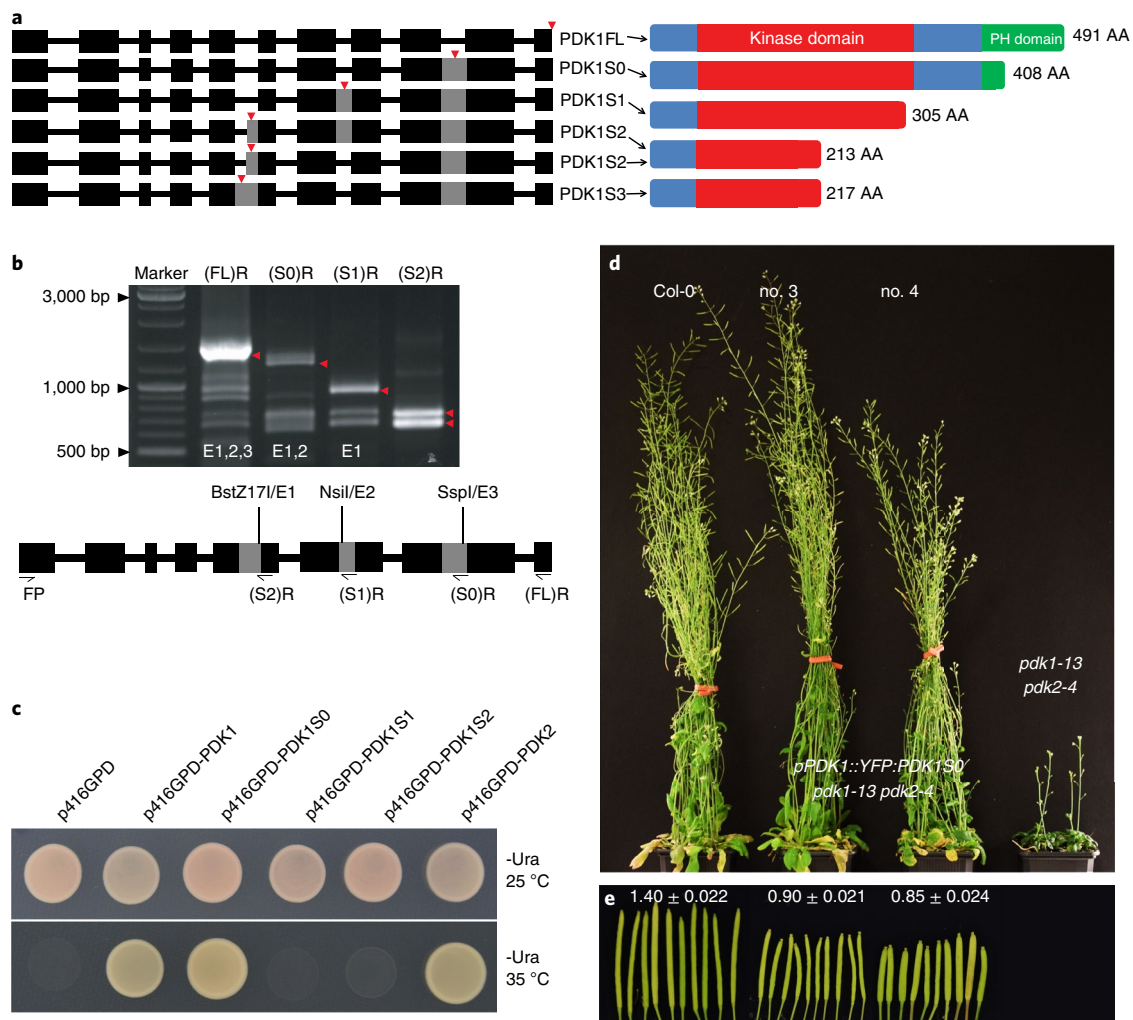


**Fig. 6 | Alternative splicing produces a *PDK1* transcript encoding a functional *PDK1* variant lacking the PH domain.** **a**, Schematic representation of the *PDK1* gene indicating the alternative splice events (left) and respective protein isoforms produced by splice variants (right). Left: wide black boxes represent exons, grey boxes represent unspliced introns, black lines represent spliced introns and red arrows indicate the locations of stop codons. Note that *PDK1S1* is lacking six amino acids of the kinase domain. **b**, Expression levels of different splice variants, as detected by RT-PCR. Similar results were obtained in four independent experiments. Primer binding and restriction enzyme recognition site locations are shown in the schematic representation below (see detailed description in Methods). Red arrowheads indicate transcripts *PDK1FL*, *PDK1S0*, *PDK1S1* and *PDK1S2/3* (from left to right) detected using the reverse primers and restriction enzymes indicated above and below the gel image, respectively. **c**, Rescue of temperature-sensitive growth of the yeast *pkh1 pkh2* mutant strain by expression of *PDK1* or *PDK2* full-length cDNA or the *PDK1S0* splice variant cDNA on the synthetic defined medium lacking uracil (-Ura). Three biological repeats showed the same result. **d, e**, The *pPDK1::YFP:PDK1S0* construct rescued the delay in flowering time, short plant height and dwarf rosette leaves of the *pdk1-13 pdk2-4* mutant (**d**, 65-day-old plants from 14 independent lines were observed), but plants developed shorter siliques carrying fewer seeds (**e**). Rescue was observed in the subsequent T2, T3 and T4 generations. **e**, Numbers above siliques represent average silique length  $\pm$  s.e.m. ( $n=10$  independent siliques).

did not completely rescue the strongly decreased lateral root development of the *pdk1 pdk2* mutant (Extended Data Fig. 8m–o). In a parallel study, Tan and co-workers showed that reduced lateral root initiation is caused by lack of activation of the *PDK1* substrates D6PK/D6PKLs<sup>34</sup>. This indicates that *PAX* has a very specific role in vascular development.

***pdk1 pdk2* cotyledon defects uncover a more general role for *PDK1* in vascular development.** The fragmented pattern of *pDR5::GUS* expression in *pdk1 pdk2* mutant cotyledons (Fig. 2k) suggested that *PDK1* and *PDK2* are also involved in vascular development in cotyledons. Compared to other known mutants with cotyledon vein defects, *pdk1 pdk2* cotyledons exhibited a unique, highly fragmented vein pattern similar to that in the mutants *scarface*

(*scf-9*) or *gnom* (*emb30-1*) (Fig. 5)<sup>35</sup>. Vascular defects were even more marked in fused *pdk1 pdk2* cotyledons, showing both vein fusion and fragmentation (Fig. 5c). Vein patterning in cotyledons was largely restored in *PAX(SD) pdk1 pdk2* seedlings, although some fragmentation and discontinued loops could be observed (Fig. 5m). We also observed that *PAX(SD) pdk1 pdk2* had relatively expanded rosette leaves in the soil compared to *pdk1 pdk2*, while *PAX pdk1 pdk2* did not (Extended Data Fig. 8p,q). These results suggested that the function of *PDK1*-mediated *PAX* activation is not limited to (pro)vascular tissues in the roots, but that it plays a more general role during vascular development.

**A *PDK1* splice variant produces a functional *PDK1* protein lacking the PH domain.** The *PDK2* gene produces a single transcript

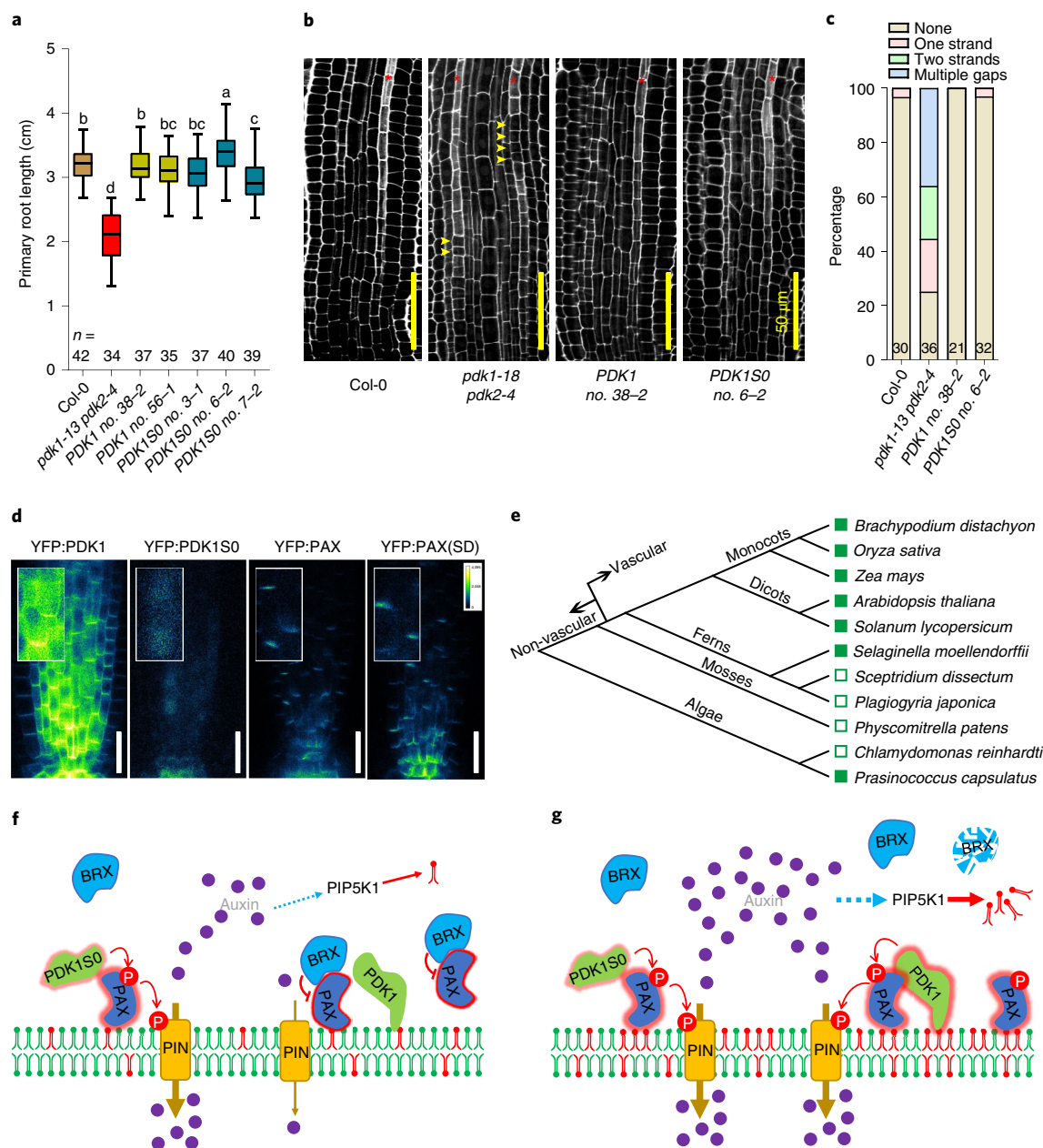


**Fig. 7 | The PH domain is not essential for PDK1 function in the auxin-sensing rheostat during vascular development. a–c**, *pdk1 pdk2* primary root length (**a**) and PPSE defects (**b,c**) are complemented by PDK150. **a**, *n* indicates the number of independent 8-day-old seedlings measured for each line; statistically different groups are indicated by lower case letters, as determined by one-way ANOVA followed by Tukey's test ( $P < 0.05$ ; details of statistical analyses are provided in Supplementary Table 4). Boxes indicate first and third quartile, horizontal lines in boxes the median, and whiskers the maximum and minimum. **b**, Red asterisks indicate the protophloem cell layer, yellow arrowheads indicate gap locations. **c**, Numbers in columns represent total counts of observed roots. **d**, Subcellular localization of YFP:PDK1, YFP:PDK150, YFP:PAX and YFP:PAX(SD) in *pdk1 pdk2* mutant stele cells. Scale bars, 20  $\mu\text{m}$ . Eight independent roots were observed for each transgenic line in a single experiment. **a–d**, Similar results were obtained in three independent experiments. **e**, Phylogenetic analysis of PDK1 protein sequences from different plant species. Solid and hollow green boxes represent PDK1 encompassing or lacking the PH domain, respectively. **f,g**, Models showing the role of PDK1 in the auxin-sensing rheostat controlling auxin efflux during root protophloem differentiation. Both membrane-localized PDK1 and the cytosolic splice variant PDK150 can phosphorylate and activate PAX. When the cellular auxin level is low, PAX is bound by BRX and this prevents its activation by PDK1 (ref. <sup>28</sup>). **f**, Only unbound PAX can be activated by PDK150 or PDK1, resulting in limited auxin efflux. As cellular auxin levels rise, BRX degradation and subcellular trafficking to the nucleus release PAX<sup>28</sup>, thereby facilitating activation of PAX by PDK1 and the subsequent promotion of auxin efflux by PAX-mediated PIN phosphorylation. **g**, In addition, auxin activates *PIP5K1* expression and stimulates the concentration of PI(4,5)P<sub>2</sub> (phospholipid in red) in the PM, resulting in enhanced PDK1 kinase activity<sup>22,38</sup>.

but, while cloning the *PDK1* full-length complementary DNA, we noticed that the *PDK1* gene produces at least six different mature transcripts due to alternative splicing events at the fifth, seventh and ninth introns (<https://www.araport.org/>). These splice variants can

be translated into five different protein isoforms, which we named respectively PDK1, PDK1S0, PDK1S1, PDK1S2 and PDK1S3 (Fig. 6a,b). Only full-length PDK1 and the PDK1S0 isoform have a complete kinase domain (Fig. 6a). To test the functionality of the

different isoforms, we expressed the corresponding complementary DNAs in yeast (*Saccharomyces cerevisiae*) strain INA106-3B. In this strain, the *PKH2* gene copy has been replaced by *LEU2* and the mutant *PKH1* gene copy encodes a thermosensitive protein allowing growth at 25 but not at 35 °C (ref. <sup>36</sup>). Expression of only those cDNAs producing full-length PDK1 or PDK2, or the PDK1S0 isoform, allowed growth at the restricted temperature, suggesting that even a small deletion of the conserved kinase domain (as is the case in PDK1S1) renders PDK1 non-functional (Fig. 6c). This is in line with the loss of function observed for the new *Arabidopsis* alleles *pdk1-11*, *-13*, *-14*, *-31* and *-32*, which all express partial PDK1 proteins having a smaller or bigger deletion of the C-terminal part of the kinase domain (Fig. 1c–e). The data on yeast were confirmed by 35S promoter-driven expression in the *Arabidopsis pdk1 pdk2* loss-of-function mutant background (Extended Data Fig. 9a). Expression of PDK1S1 and PDK1S2 did not result in any phenotypic rescue (Extended Data Fig. 9a), whereas expression of a cytosolic-localized YFP:PDK1S0 fusion under control of the *PDK1* promoter completely rescued the vegetative growth defects of the mutant (Fig. 6d and Extended Data Fig. 9a–c). Upon flowering, however, *pPDK1::YFP:PDK1S0 pdk1-14 pdk2-4* plants developed shorter siliques carrying fewer seeds compared to wild-type plants (Fig. 6e). This silique phenotype has also been described for the *pdk1-b pdk2-1* double mutant<sup>14</sup> and, according to our own analysis, the T-DNA insertion in the *pdk1-b* allele leads to the production of a shorter PDK1 protein with an intact kinase domain but lacking the PH domain (Supplementary Fig. 1).

Interestingly, the *pPDK1::YFP:PDK1S0* construct also rescued primary root and cotyledon vein defects of the *pdk1 pdk2* mutant (Fig. 5m and Extended Data Fig. 8g–i). Because PDK1S0 localized to the cytosol, this indicated that PH domain-directed basal PDK1 localization is not essential for vascular development (Fig. 7a–d and Extended Data Fig. 9b,c). Moreover, both YFP:PAX and YFP:PAX(SD) localized to the basal (rootward) plasma membrane in the *pdk1 pdk2* mutant background, indicating that PAX basal localization is not dependent on its interaction with PDK1, nor on its phosphorylation status (Fig. 7d). Most likely, PAX provides a co-localization and interaction site for PDK1S0 at the basal side of root protophloem cells, and possibly the higher kinase activity of the PDK1S0 version (Extended Data Fig. 9d) can compensate for the lack of immediate co-localization with the PAX substrate.

The PH domain has been proposed to be characteristic for PDK1 in vascular plant species<sup>9</sup>. Based on our results, however, we re-examined PDK1 protein sequences in several non-vascular and vascular plants. Although all flowering plant PDK1 proteins contain a C-terminal PH domain, PDK1 proteins in certain ferns (*Sceptridium dissectum* and *Plagiogyria japonica*) do not, while these species do develop vascular tissue. Interestingly, the PDK1 orthologue of the green alga *Prasinococcus capsulatus* does have a PH domain (Fig. 7e), suggesting that the ancestral plant PDK1 had a PH domain and that this domain has been lost in some early non-seed plant classes but maintained in flowering plants. In conclusion, this evolutionary analysis shows that the PH domain in PDK1 is not specific to vascular plants.

## Discussion

*PDK1* loss-of-function mutations cause lethality in yeasts and animals<sup>3,5,10,11</sup>. However, the previously reported impact of loss of function of *PDK1* in plants was only limited<sup>8,12–15</sup>. In this study, we show that *pdk1 pdk2* loss of function results in strong developmental defects in *Arabidopsis*. Different from yeasts and animals though, and more similar to the situation in *P. patens*, *Arabidopsis pdk1 pdk2* loss-of-function mutants are viable. The fact that both PDK1 and PDK2 can complement a yeast *pdk* mutant suggests not that substrate specificity has changed, but that the downstream targets of PDK1 have lost their involvement in signalling pathways that are

essential for cell survival. Previously, PID has been proposed to be a key substrate of PDK1 (ref. <sup>16</sup>). However, this was based purely on in vitro data and, since *pdk1 pdk2* mutants did not share the pin-formed inflorescence and aberrant flower phenotypes that are typical for *pid* loss-of-function mutants, we concluded that PDK1 appears not to be essential for PID function in these tissues. PID is an auto-activating kinase in vitro and might act independent of upstream activating kinases<sup>20,21</sup>, or other kinases than PDK1 might be involved in hyperactivating PID during embryo, inflorescence and flower development. The latter seems most likely based on the observation that flower, leaf and shoot extracts can hyperactivate PID in vitro<sup>16</sup>. A physical interaction between PID and PDK1 through the PIF domain, as suggested by Zegzouti and co-workers<sup>16</sup>, has never been proved, and was based purely on in vitro phosphorylation data. Here we show unequivocally that PID does not require PDK1 for its association with the PM, which corroborates the finding that this is mediated by an arginine-rich loop in the kinase domain of PID<sup>37</sup>. All data are in line with the observation that a PID:GUS fusion lacking the PIF domain can still complement *pid* loss-of-function mutants<sup>21</sup>.

Our data indicate a role for PDK1 as positive regulator of polar auxin transport, upstream of several AGC1 clade kinases. As an example, we selected the AGC1 kinase PAX and show that PDK1 is part of an auxin-sensing molecular rheostat that controls polar auxin transport during vascular development in roots and cotyledons. PAX is central to this rheostat, because it enhances auxin efflux by phosphorylating PIN proteins in their large hydrophilic loop (Fig. 7f,g). At low auxin levels PAX activation by PDK1 is prevented by BRX binding, resulting in limited auxin efflux (Fig. 7f). As a consequence, auxin levels in the cell rise, leading to dissociation of BRX and thereby allowing PDK1 to promote auxin efflux by activating PAX via phosphorylation (Fig. 7g). In our work, *PDK1* expression was not responsive to auxin treatment (Extended Data Fig. 10a). However, auxin is known to induce expression of the *PHOSPHATIDYLINOSITOL 4-PHOSPHATE 5-KINASE 1* (*PIP5K1*) gene, resulting in increased PI(4,5)P<sub>2</sub> levels<sup>38</sup>. We clearly observed that YFP:PDK1 shifted from the PM to cytosol after treatment with the phospholipid biosynthesis inhibitors wortmannin and phenylarsine oxide (Extended Data Fig. 10b,d,e). This implies that PDK1 PM localization is dependent on phospholipid accumulation on the PM, and that auxin treatment might promote the recruitment of PDK1 to the PM. In our work, however, auxin treatment did not significantly enhance PDK1 basal PM localization in root stele cells (Extended Data Fig. 10b,c). This suggests, indirectly, that phospholipids might be rate limiting for either PAX polarity or PDK1 kinase activity<sup>22</sup>. The similarities in cotyledon vein fragmentation among mutants *pdk1 pdk2*, *cvp2 cvl1* and *pip5k1 pip5k2* (Fig. 5g,h) suggest that phospholipids are part of the auxin transport-controlling regulatory pathway. Most likely they are necessary for the PM association of PAX and of other AGC1 clade kinases<sup>34</sup> downstream of PDK1. Moreover, since the PDK1S0 isoform is clearly more active than full-length PDK1 in auto- and transphosphorylation in vitro (Extended Data Fig. 9d), alternative splicing of *PDK1* transcripts might provide a mechanism for balancing the phospholipid requirement of PDK1 activity under specific growth conditions or in certain developmental processes.

## Methods

**Plant lines and growth conditions.** *Arabidopsis thaliana* (L.) ecotype Columbia 0 (Col-0) was used as wild-type control for all experiments because all mutant and transgenic lines are in the Col-0 background. Previously described T-DNA insertion lines SALK\_053385 (*pdk1.1-1*, renamed *pdk1-c*), SALK\_113251C (*pdk1.1a*, renamed *pdk1-a*), SALK\_007800 (*pdk1.1b*, renamed *pdk1-b*), SAIL\_62\_G04 (*pdk1.2-2*, renamed *pdk2-4*) and SAIL\_450\_B01 (*pdk1.2-3*, renamed *pdk2-1*) were obtained from the Nottingham Arabidopsis Stock Centre<sup>14,15</sup> (Supplementary Table 2). The following additional *Arabidopsis* lines are described elsewhere: *sfc-9* (SALK\_069166)<sup>39</sup>, *gnom/emb30-1* (CS6320)<sup>40</sup>, *pip5k1 pip5k2* (ref. <sup>38</sup>), *cvp2 cvl1* (ref. <sup>41</sup>), *d6pk012* (ref. <sup>24</sup>), *pin1* (SALK\_047613)<sup>42</sup>, *tir1-1 afb1-3 afb2-3 afb3-4* (ref. <sup>43</sup>), *arf5-1* (SALK\_023812)<sup>44</sup>, *pDR5::GFP* (ref. <sup>45</sup>), *pDR5::GUS*<sup>21</sup>, *pPIN1::PIN1:GFP*<sup>45</sup>, *pPIN2::PIN2:GFP*<sup>46</sup>, *pPIN3::PIN3:GFP*<sup>47</sup>, *pPIN7::PIN7:GFP*<sup>48</sup>

and *p35S::PID no. 21* (ref. <sup>21</sup>). For lines created in this study, T-DNA constructs *p35S::YFP-PDK1*, *p35S::PDK1*, *pPDK1/2::turboGFP:GUS* and *pYAO-Cas9-gRNA1/2/3* were transformed into Col-0 using *Agrobacterium*-mediated floral dip transformation<sup>49</sup>. Homozygous lines with a single T-DNA insertion were selected for further analysis. Of the 80 CRISPR/Cas9 transgenic alleles obtained, seven appeared to contain loss-of-function mutations in the third and seventh exons of *PDK1*. The CRISPR/Cas9 T-DNA construct in the new *pdk1* mutant alleles was segregated during the generation of the *pdk1 pdk2* double mutant. Five mutant alleles with open-reading frame shifts were used for further analysis (Fig. 1c,d).

For complementation analysis of PDK1 isoforms and PAX, one of the T-DNA constructs *p35S::YFP-PDK1* and *p35S::PDK1FL/S1/S2* was transformed into the *pdk1-13(±) pdk2-4(-/-)* mutant background; *p35S::YFP-PDKS0* or *p35S::PDK1S0* was transformed into the *pdk1-13(-/-) pdk2-1(±)* mutant background; and *pPDK1::YFP-PDK1FL/PAX/PAX(S596D)* or *pPDK1::YFP-PDK1S0* was transformed into the *pdk1-14(-/-) pdk2-4(±)* or *pdk1-13(±) pdk2-4(-/-)* mutant background, respectively. The genotype of the *pdk1 pdk2* mutant background was confirmed by PCR before floral dip transformation. The genotyping primers are summarized in Supplementary Table 3.

Plants were grown in soil at 21 °C, 16-h photoperiod and 70% relative humidity. For seedling growth, seeds were surface-sterilized for 1 min in 70% ethanol and 10 min in 1% chlorine followed by five washes with sterile water. Sterilized seeds were kept in the dark at 4 °C for 2 d for vernalization and germinated on vertical plates with 0.5× Murashige and Skoog (1/2 MS) medium (Duchefa) containing 0.05% MES, 0.8% agar and 1% sucrose at 22 °C and 16-h photoperiod.

**RNA extraction and RT-qPCR.** Total RNA was extracted from 5-day-old seedlings using a NucleoSpin RNA Plant kit (Macherey Nagel, no. 740949). Reverse transcription was performed using a RevertAid Reverse Transcription Kit (Thermo Scientific, no. K1691). For RT-qPCR on auxin-induced genes, RNA was isolated from 5-day-old Col-0 and *pdk1-13 pdk2-4* seedlings treated for 1 h with 10 μM IAA. Gene expression was normalized to the reference gene *PP2A-3 (AT2G42500)* using the  $\Delta\Delta C_q$  method. For analysis of *pdk1* and *pdk2* T-DNA alleles, RT-qPCR was performed with DreamTaq DNA Polymerases (Thermo Scientific). RT-qPCR primers are listed in Supplementary Table 3. For detection of *PDK1* splice variants, RT-PCR was performed for 40 cycles using the forward (FP) and reverse (FL, S0, S1 and S2) primers (Fig. 6b) listed in Supplementary Table 3. PCR reactions with the primer pair FP and (FL)R were digested with *BstZ171*, *NsiI* and *SspI* to detect *PDK1FL*, with primer pair FP and (S0)R with *BstZ171* and *NsiI* to detect *PDK1S0*, and with primer pair FP and (S1)R with *BstZ171* to detect *PDK1S1*. Next, 0.1 μl of the enzymes *BstZ171*, *NsiI* and/or *SspI* (Thermo Scientific) was directly added to the 20-μl PCR reaction and reactions were incubated at 37 °C overnight before gel electrophoresis. Detection of *PDK1S2* and *PDK1S3* with primer pair FP and (S2) R did not require restriction enzyme digestion. RT-qPCR was performed with the CFX96 Touch Real-Time PCR Detection System (Bio-Rad) using TB Green Premix Ex Taq II (Tli RNase H Plus) (Takara, no. RR820B).

**Cloning procedures.** To generate the *Promoter::turboGFP:GUS* fusions, a *SacI-TurboGFP-PacI* fragment was cloned from *pICSL80005* into *pMDC163* (ref. <sup>50</sup>), resulting in *pMDC163(gateway)-TurboGFP:GUS*. *PDK1* and *PDK2* promoter regions of approximately 2.0 kb, including the first six codons, were amplified from Col-0 genomic DNA using the primers listed in Supplementary Table 3, and cloned in *pDONR207* by LR recombination. The resulting fragments were subsequently fused in-frame with the *turboGFP:GUS* reporter gene in *pMDC163(gateway)-TurboGFP:GUS* by BP recombination (Gateway BP/LR Clonase II Enzyme Mix, Invitrogen, nos. 11789020 and 12538120).

*PDK1* splice variants were amplified from cDNA of 5-day-old seedlings using the respective primers (Supplementary Table 3), after which the restriction enzymes described for RT-qPCR were employed. Fragments were cloned in *pDONR207* by BP recombination and subsequently transferred to *pART7-35S::YFP:gateway* by LR recombination<sup>51</sup>, resulting in *pART7-35S::YFP:PDK1FL/S0/S1/S2*. Expression cassettes were excised with *NotI* and cloned into *NotI*-digested *pART27*, resulting in *pART27-35S::YFP:PDK1FL/S0*. The same entry vectors and LR recombination were used to generate *pMDC32-35S::PDK1FL/S0/S1/S2*, *pGEX-PDK1FL/S0*, *pGEX-PIN1HL*, *pGEX-PIN2HL* and *p35S::PID:YFP* have been described previously<sup>19,52,53</sup>. *PIN3HL*, *PIN7HL* and *PAX* were amplified from Col-0 cDNA using the primers listed in Supplementary Table 3, and cloned into *pGEX* also using Gateway cloning technology to obtain *pGEX-PIN3HL*, *-PIN7HL* and *-PAX*.

To generate *pPDK1::YFP:PDK1FL/PDK1S0/PAX/PAX(S596D)* fusions, the 2.0-kb *PDK1* promoter region was introduced into *pART27-35S::YFP:PDK1S0* by replacing the 35S sequence using restriction enzymes *BstXI* and *KpnI*. *pART27-pPDK1::YFP:PDK1S0* and *pDONR207* were mixed with BP clonase to obtain *pART27-pPDK1::YFP:gateway*. *PDK1FL* was then recombined into *pART27-pPDK1::YFP:gateway* by LR reaction to obtain *pART27-pPDK1::YFP:PDK1FL*. *PAX* was amplified from Col-0 cDNA and cloned into *pDONR207* and the entry vector was mutated with the QuickChange II XL Site-Directed Mutagenesis Kit (Agilent, no. 200521). *PAX* and *PAX(S596D)* were then also introduced into *pART27-pPDK1::YFP:gateway* by LR reaction.

To obtain the *p416GPD-PDK* constructs for expression in yeast, *BamHI-PDK1FL/S0/S1/S2-EcoRI* and *BamHI-PDK2-XhoI* fragments were amplified from *pDONR207-PDK1FL/S0/S1/S2* and 5-day-old seedling cDNA, respectively, using the primers listed in Supplementary Table 3. Fragments were digested with the appropriate restriction enzymes and ligated into vector *p416GPD*<sup>54</sup>.

The *pCambia-pYAO-Cas9-gRNA1/2/3* plasmids for CRISPR/Cas9-mediated mutagenesis were obtained by ligating the *EcoRI*-(Cas9 + terminator)-*AvrII* fragment from *pDE-Cas9* (ref. <sup>55</sup>) into *pCambia1300* digested with *EcoRI* and *XbaI*. The *EcoRI* and *SalI* sites in the resulting *pCambia-Cas9* plasmid were used to clone the *EcoRI*-*YAO* promoter-*EcoRI*<sup>56</sup> and *XhoI*-gateway-*XhoI* fragments amplified from, respectively, *Arabidopsis* Col-0 gDNA and the *pART7-35S::YFP:gateway* plasmid. Regions producing gRNAs (Supplementary Table 3) designed to target, respectively, the third, sixth or seventh exon of *PDK1* were ligated into *pEn-Chimera*<sup>55</sup> and introduced behind the *YAO* promoter in *pCambia-pYAO-Cas9-gateway* by LR recombination.

All primers used for cloning are summarized in Supplementary Table 3.

**General phenotypic analysis and physiological experiments.** NPA-treated (stock in dimethylsulfoxide (DMSO), 1:10<sup>4</sup> dilution), normally or dark-grown grown seedlings, potted plants, siliques and inflorescences were photographed with a Nikon D5300 camera at the indicated times. For imaging of inflorescences, the top part of the inflorescence was cut from 15-cm-high plants. For Fig. 2a, seedlings were transferred to and aligned on a black plate before imaging. Primary root length, rosette diameter, silique length and hypocotyl curvature under directional light treatment were measured with ImageJ (Fiji). Plant height was measured directly using a ruler. Root tips, apical hook, opened siliques, flowers, details of floral organs and cotyledons were imaged using a Leica MZ16FA stereomicroscope equipped with a Leica DFC420C camera. All measurements based on photographs were performed in ImageJ and analysed and plotted into graphs in GraphPad Prism 5.

**Phenotypic analysis of reproductive organs and vascular development.** To examine pollen vitality, anthers were collected from flowers just before opening into 70 μl Alexander staining buffer (10% ethanol, 0.01% (w/v) malachite green, 25% glycerol, 5% (w/v) phenol, 5% (w/v) chloral hydrate, 0.05% (w/v) fuchsin acid, 0.005% (w/v) OrangeG and 1.5% glacial acetic acid) on a microscopy slide, covered with a coverslip and incubated at 55 °C for 1 h before imaging. For pollen tube growth, pollen of recently opened flowers was transferred to a dialysis membrane placed on solid pollen germination medium (18% sucrose, 0.01% boric acid, 1 mM CaCl<sub>2</sub>, 1 mM Ca(NO<sub>3</sub>)<sub>2</sub>, 1 mM MgSO<sub>4</sub> and 0.5% agarose) and incubated at 22 °C for 18 h. Ovules were cleared in chloral hydrate solution (chloral hydrate:glycerol:water, 4:2:1 by weight) for 4 h. Stained or germinated pollen and cleared ovules were imaged using a Zeiss Axioplan 2 microscope with DIC optics and Zeiss AxioCam MRC5 digital colour camera. Pollen tube length was measured with ImageJ (Fiji).

For observation of cotyledon vein patterns, 5-day-old seedlings were cleared in 70% ethanol overnight and placed on slides with the chloral hydrate solution mentioned above for 2-d clearing. A Leica MZ16FA fluorescence stereomicroscope equipped with a Leica DFC420C camera was used for photography.

The modified pseudo-Schiff-propidium iodide (PI) method was employed to stain the cell walls of 5-day-old seedling roots for protophloem observation and quantification<sup>57</sup>. PI was excited with a 488-nm laser and the emission signal was collected using a 600-nm long-pass filter using a Zeiss LSM5 Exciter/Axiomager. To quantify gap types, one gap from both strands or more than one gap from both strands were classified into 'two strands' or 'multiple gaps' groups, respectively.

**Protoplast isolation and transformation.** Protoplasts were isolated and transformed as previously described, but with certain modifications to the protocol<sup>58</sup>. Protoplasts were isolated from 4-week-old rosette leaves rather than from cell suspensions, and we used a 40% PEG4000 solution and 15 μg of *pART7-35S::PID:YFP* for each transformation.

**Auxin transport measurements.** Auxin transport assays were carried out as previously reported, with certain modifications<sup>54</sup>. Four 2.5-cm inflorescence stem segments from the basal part of 15-cm inflorescence stems were placed in inverted orientation in 30 μl of auxin transport buffer (0.5 nM IAA, 1% sucrose, 5 mM MES, pH 5.5) with or without 50 μM NPA for 1 h, then transferred to 30 μl of auxin transport buffer with or without 50 μM NPA containing 200 nM radiolabelled [<sup>3</sup>H]IAA (Scopus Research), allowed to incubate for 30 min and subsequently transferred to 30 μl of auxin transport buffer without radiolabelled [<sup>3</sup>H]IAA and incubated for another 4 h. Segments were cut into 5-mm pieces, the bottom piece (0–5 mm) was discarded and the remaining pieces were placed separately into 5 ml of Ultima Gold (PerkinElmer, no. 6013329) for overnight maceration. [<sup>3</sup>H]IAA was quantified using a PerkinElmer Tri-Carb 2810TR low-activity liquid scintillation analyser.

**GUS staining and microscopy.** Fresh seedlings and plant organs were directly soaked in GUS staining buffer (10 mM EDTA, 50 mM sodium phosphate

(pH 7.0), 0.1% (v/v) Triton X-100, 0.5 mM  $K_3Fe(CN)_6$ , 0.5 mM  $K_4Fe(CN)_6$ , 1 mg ml<sup>-1</sup> 5-bromo-4-chloro-3-indolyl-D-glucuronide) under vacuum for 15 min and incubated at 37°C for 18 h. Subsequently, samples were cleared in 70% (v/v) ethanol at room temperature before imaging with either a Leica MZ16FA or Leica MZ12 fluorescence stereomicroscope equipped with a Leica DFC420C or DC500 camera, respectively.

To visualize YFP:PDK1 in embryos and roots or PID:YFP in protoplasts, a Zeiss LSM5 Exciter/Axiomager equipped with a 514-nm laser and 530–560-nm band-pass filter was used. GFP signals in roots of 5-day-old seedlings were visualized by optionally staining with 10 µg ml<sup>-1</sup> PI for 5 min on slides, and samples were observed with a Zeiss LSM5 Exciter/Axiomager equipped with a 488-nm laser and a 505–530 nm band-pass filter to detect GFP fluorescence, or a 650-nm long-pass filter to detect PI fluorescence. All images were captured with a ×40/1.2 numerical aperture oil immersion objective. For PH domain-dependent PDK1 subcellular localization analysis, 4-day-old seedlings were treated with 0.1% DMSO, 33 µM wortmannin (Sigma-Aldrich, no. W1628) or 1 µM IAA (Duchefa Biochemie, no. I0901) for 1 h or 30 µM phenylarsine oxide (Sigma-Aldrich, no. P3075) for 30 min in 1/2 MS liquid media before microscopic observation.

Images were optimized in Adobe Photoshop cc2018 and assembled into figures using Adobe Illustrator cc2017. *pDR5::GFP* total intensity was measured from three-dimensional reconstruction of the root tips with ImageJ (Fiji). Apical PIN2:GFP abundance was also measured with ImageJ (Fiji) by drawing a freehand line along the centre of the apical PM of epidermal cells.

**Phylogenetic analysis.** Protein sequences of *PDK1* homologous genes from the following species were obtained from the National Center for Biotechnology Information: *Solanum lycopersicum* (Gene ID: 544184), *Zea mays* (Gene ID: 100384040), *Oryza sativa* (Gene ID: 4324953), *Brachypodium distachyon* (Gene ID: 100835821), *P. patens* (Gene ID: 112277681), *Selaginella moellendorffii* (Gene ID: 9631841), *Chlamydomonas reinhardtii* (Gene ID: 5726920) and *A. thaliana* (Gene ID: 830330). The three remaining PDKs, from *P. japonica* (onekp:UWOD\_scaffold\_2139095), *S. dissectum* (onekp:EAAQ\_scaffold\_2087606) and *P. capsulatus* (onekp:XMCL\_scaffold\_2001871), which had only incomplete N-terminal information, were obtained from data for the 1,000 Plants project (<http://www.onekp.com>). Eleven sequences were aligned by ClustalW in MEGA-X, and a phylogenetic tree was then constructed using the maximum-likelihood procedure. Concomitantly, protein secondary structures were predicted by the InterPro online tool, <https://www.ebi.ac.uk/interpro/>.

**In vitro phosphorylation and yeast complementation.** In vitro phosphorylation and yeast complementation experiments were performed as previously described<sup>8,52</sup>.

**Reporting Summary.** Further information on research design is available in the Nature Research Reporting Summary linked to this article.

## Data availability

All processed data are contained either in the manuscript, Extended Data or Supplementary Information. Raw data and materials generated during this study are available upon reasonable request.

Received: 20 September 2019; Accepted: 25 March 2020;

Published online: 11 May 2020

## References

- Biondi, R. M. et al. Identification of a pocket in the PDK1 kinase domain that interacts with PIF and the C-terminal residues of PKA. *EMBO J.* **19**, 979–988 (2000).
- Frödin, M. et al. A phosphoserine/threonine-binding pocket in AGC kinases and PDK1 mediates activation by hydrophobic motif phosphorylation. *EMBO J.* **21**, 5396–5407 (2002).
- Mora, A., Komander, D., Van Aalten, D. M. F. & Alessi, D. R. PDK1, the master regulator of AGC kinase signal transduction. *Semin. Cell Dev. Biol.* **15**, 161–170 (2004).
- Bayascas, J. R. in *Phosphoinositide 3-kinase in Health and Disease. Current Topics in Microbiology and Immunology* Vol. 346 (eds Rommel C., Vanhaesebroeck B. et al.) 9–29 (2010).
- Casamayor, A., Torrance, P. D., Kobayashi, T., Thorner, J. & Alessi, D. R. Functional counterparts of mammalian protein kinases PDK1 and SGK in budding yeast. *Curr. Biol.* **9**, 186–197 (1999).
- Niederberger, C. & Schweingruber, M. E. A *Schizosaccharomyces pombe* gene, *ksg1*, that shows structural homology to the human phosphoinositide-dependent protein kinase PDK1, is essential for growth, mating and sporulation. *Mol. Gen. Genet.* **261**, 177–183 (1999).
- Voordeckers, K. et al. Yeast 3-phosphoinositide-dependent protein kinase-1 (PDK1) orthologs Pkh1–3 differentially regulate phosphorylation of protein kinase A (PKA) and the protein kinase B (PKB)/S6K ortholog Sch9. *J. Biol. Chem.* **286**, 22017–22027 (2011).
- Dittrich, A. C. N. & Devarenne, T. P. Characterization of a PDK1 homologue from the moss *Physcomitrella patens*. *Plant Physiol.* **158**, 1018–1033 (2012).
- Dittrich, A. C. N. & Devarenne, T. P. Perspectives in PDK1 evolution: Insights from photosynthetic and non-photosynthetic organisms. *Plant Signal. Behav.* **7**, 642–649 (2012).
- Lawlor, M. A. et al. Essential role of PDK1 in regulating cell size and development in mice. *EMBO J.* **21**, 3728–3738 (2002).
- Rintelen, F., Stocker, H., Thomas, G. & Hafen, E. PDK1 regulates growth through Akt and S6K in *Drosophila*. *Proc. Natl Acad. Sci. USA* **98**, 15020–15025 (2002).
- Devarenne, T. P., Ekengren, S. K., Pedley, K. F. & Martin, G. B. Adi3 is a Pdk1-interacting AGC kinase that negatively regulates plant cell death. *EMBO J.* **25**, 255–265 (2006).
- Matsui, H., Miyao, A., Takahashi, A. & Hirochika, H. Pdk1 kinase regulates basal disease resistance through the OsOx1-OsPti1a phosphorylation cascade in rice. *Plant Cell Physiol.* **51**, 2082–2091 (2010).
- Camehl, I. et al. The OXI1 kinase pathway mediates *Piriformospora indica*-induced growth promotion in *Arabidopsis*. *PLoS Pathog.* **7**, e1002051 (2011).
- Scholz, S. et al. The AGC protein kinase UNICORN controls planar growth by attenuating PDK1 in *Arabidopsis thaliana*. *PLoS Genet.* **15**, e1007927 (2019).
- Zegzouti, H., Anthony, R. G., Jahchan, N., Bogre, L. & Christensen, S. K. Phosphorylation and activation of PINOID by the phospholipid signaling kinase 3-phosphoinositide-dependent protein kinase 1 (PDK1) in *Arabidopsis*. *Proc. Natl Acad. Sci. USA* **103**, 6404–6409 (2006).
- Zegzouti, H. et al. Structural and functional insights into the regulation of *Arabidopsis* AGC VIIa kinases. *J. Biol. Chem.* **281**, 35520–35530 (2006).
- Gray, J. W. et al. Two Pdk1 phosphorylation sites on the plant cell death suppressor Adi3 contribute to substrate phosphorylation. *Biochim. Biophys. Acta* **1834**, 1099–1106 (2013).
- Galván-Ampudia, C. S. & Offringa, R. Plant evolution: AGC kinases tell the auxin tale. *Trends Plant Sci.* **12**, 541–547 (2007).
- Christensen, S. K., Dagenais, N., Chory, J. & Weigel, D. Regulation of auxin response by the protein kinase PINOID. *Cell* **100**, 469–478 (2000).
- Benjamins, R., Quint, A., Weijers, D., Hooykaas, P. & Offringa, R. The PINOID protein kinase regulates organ development in *Arabidopsis* by enhancing polar auxin transport. *Development* **128**, 4057–4067 (2001).
- Anthony, R. G. et al. A protein kinase target of a PDK1 signalling pathway is involved in root hair growth in *Arabidopsis*. *EMBO J.* **23**, 572–581 (2004).
- Anthony, R. G., Khan, S., Costa, J., Pais, M. S. & Bögre, L. The *Arabidopsis* protein kinase PTII-2 is activated by convergent phosphatidic acid and oxidative stress signaling pathways downstream of PDK1 and OXI1. *J. Biol. Chem.* **281**, 37536–37546 (2006).
- Zourelidou, M. et al. The polarly localized D6 PROTEIN KINASE is required for efficient auxin transport in *Arabidopsis thaliana*. *Development* **136**, 627–636 (2009).
- Won, S.-K. et al. cis-Element- and transcriptome-based screening of root hair-specific genes and their functional characterization in *Arabidopsis*. *Plant Physiol.* **150**, 1459–1473 (2009).
- Zhang, Y., He, J. & McCormick, S. Two *Arabidopsis* AGC kinases are critical for the polarized growth of pollen tubes. *Plant J.* **58**, 474–484 (2009).
- Li, E. et al. AGC1.5 kinase phosphorylates ROPGEFs to control pollen tube growth. *Mol. Plant* **11**, 1198–1209 (2018).
- Marhava, P. et al. A molecular rheostat adjusts auxin flux to promote root protophloem differentiation. *Nature* **558**, 297–300 (2018).
- Friml, J. et al. A PINOID-dependent binary switch in apical-basal PIN polar targeting directs auxin efflux. *Science* **306**, 862–865 (2004).
- Sabatini, S. et al. An auxin-dependent distal organizer of pattern and polarity in the *Arabidopsis* root. *Cell* **99**, 463–472 (1999).
- Bao, F. et al. Brassinosteroids interact with auxin to promote lateral root development in *Arabidopsis*. *Plant Physiol.* **134**, 1624–1631 (2004).
- Willige, B. C. et al. D6PK AGCVIII kinases are required for auxin transport and phototropic hypocotyl bending in *Arabidopsis*. *Plant Cell* **25**, 1674–1688 (2013).
- Haga, K., Frank, L., Kimura, T., Schwechheimer, C. & Sakai, T. Roles of AGCVIII kinases in the hypocotyl phototropism of *Arabidopsis* seedlings. *Plant Cell Physiol.* **59**, 1060–1071 (2018).
- Tan, S. et al. A lipid code-dependent phosphoswitch directs PIN-mediated auxin efflux in *Arabidopsis* development. Preprint at *bioRxiv* <http://doi.org/10.1101/755504> (2019).
- Richter, S. et al. Role of the GNOM gene in *Arabidopsis* apical-basal patterning—from mutant phenotype to cellular mechanism of protein action. *Eur. J. Cell Biol.* **89**, 138–144 (2010).
- Inagaki, M. et al. PDK1 homologs activate the Pkc1-mitogen-activated protein kinase pathway in yeast. *Mol. Cell Biol.* **19**, 8344–8352 (1999).
- Simon, M. L. A. et al. A PtdIns(4)P-driven electrostatic field controls cell membrane identity and signalling in plants. *Nat. Plants* **2**, 16089 (2016).

38. Tejos, R. et al. Bipolar plasma membrane distribution of phosphoinositides and their requirement for auxin-mediated cell polarity and patterning in *Arabidopsis*. *Plant Cell* **26**, 2114–2128 (2014).
39. Sieburth, L. E. et al. SCARFACE encodes an ARF-GAP that is required for normal auxin efflux and vein patterning in *Arabidopsis*. *Plant Cell* **18**, 1396–1411 (2006).
40. Patton, D. A., Franzmann, L. H. & Meinke, D. W. Mapping genes essential for embryo development in *Arabidopsis thaliana*. *Mol. Gen. Genet.* **227**, 337–347 (1991).
41. Carland, F. & Nelson, T. CVP2- and CVL1-mediated phosphoinositide signaling as a regulator of the ARF GAP SFC/VAN3 in establishment of foliar vein patterns. *Plant J.* **59**, 895–907 (2009).
42. Furutani, M. PIN-FORMED1 and PINOID regulate boundary formation and cotyledon development in *Arabidopsis embryogenesis*. *Development* **131**, 5021–5030 (2004).
43. Parry, G. et al. Complex regulation of the TIR1/AFB family of auxin receptors. *Proc. Natl Acad. Sci. USA* **106**, 22540–22545 (2009).
44. Okushima, Y. et al. Functional genomic analysis of the AUXIN RESPONSE FACTOR gene family members in *Arabidopsis thaliana*: unique and overlapping functions of ARF7 and ARF19. *Plant Cell* **17**, 444–463 (2005).
45. Benkova, E., Michniewicz, M., Sauer, M., Teichmann, T. & Pflanz, M. Der Local, efflux-dependent auxin gradients as a common module for plant organ formation. *Cell* **115**, 591–602 (2003).
46. Xu, J. & Scheres, B. Dissection of *Arabidopsis* ADP-RIBOSYLATION FACTOR 1 function in epidermal cell polarity. *Plant Cell* **17**, 525–536 (2005).
47. Zádňíková, P. et al. Role of PIN-mediated auxin efflux in apical hook development of *Arabidopsis thaliana*. *Development* **137**, 607–617 (2010).
48. Bilou, I. et al. The PIN auxin efflux facilitator network controls growth and patterning in *Arabidopsis* roots. *Nature* **433**, 39–44 (2005).
49. Clough, S. J. & Bent, A. F. Floral dip: a simplified method for *Agrobacterium*-mediated transformation of *Arabidopsis thaliana*. *Plant J.* **16**, 735–743 (1998).
50. Curtis, M. D. & Grossniklaus, U. A gateway cloning vector set for high-throughput functional analysis of genes in planta. *Plant Physiol.* **133**, 462–469 (2003).
51. Gleave, A. P. A versatile binary vector system with a T-DNA organisational structure conducive to efficient integration of cloned DNA into the plant genome. *Plant Mol. Biol.* **20**, 1203–1207 (1992).
52. Huang, F. et al. Phosphorylation of conserved PIN motifs directs *Arabidopsis* PIN1 polarity and auxin transport. *Plant Cell* **22**, 1129–1142 (2010).
53. Dhonukshe, P. et al. Plasma membrane-bound AGC3 kinases phosphorylate PIN auxin carriers at TPRXS(N/S) motifs to direct apical PIN recycling. *Development* **137**, 3245–3255 (2010).
54. Mumberg, D., Müller, R. & Funk, M. Yeast vectors for the controlled expression of heterologous proteins in different genetic backgrounds. *Gene* **156**, 119–122 (1995).
55. Fauser, F., Schiml, S. & Puchta, H. Both CRISPR/Cas-based nucleases and nickases can be used efficiently for genome engineering in *Arabidopsis thaliana*. *Plant J.* **79**, 348–359 (2014).
56. Yan, L. et al. High-efficiency genome editing in *Arabidopsis* using YAO promoter-driven CRISPR/Cas9 system. *Mol. Plant* **8**, 1820–1823 (2015).
57. Truernit, E. et al. High-resolution whole-mount imaging of three-dimensional tissue organization and gene expression enables the study of phloem development and structure in *Arabidopsis*. *Plant Cell* **20**, 1494–1503 (2008).
58. Schirawski, J., Planchais, S. & Haenni, A. L. An improved protocol for the preparation of protoplasts from an established *Arabidopsis thaliana* cell suspension culture and infection with RNA of turnip yellow mosaic tymovirus: a simple and reliable method. *J. Virol. Methods* **86**, 85–94 (2000).

## Acknowledgements

We thank A. Rodriguez-Villalon, C. Hardtke, C. Schwechheimer, I. Heilmann and J. Chang (Jia Li's laboratory) for providing mutants *cvp2 cvl1*, *pax paxl*, *d6pk012*, *pip5k1 pip5k2* and *gnom*, respectively. We thank T. Devarenne for providing yeast strain *p416GPD*, S. de Pater for providing the CRISPR/Cas9 plasmids, X. Men for sharing preliminary data on PIN2HL phosphorylation by PDK1, K. Boot for help with auxin transport assays and G. Lamers and J. Willemsse for help with microscopy. We are grateful to N. Surtel, W. de Winter and J. Vink for their help with plant growth and media preparation. This project was supported by the China Scholarship Council.

## Author contributions

Y.X. and R.O. conceived the project, designed experiments and analysed and interpreted results. Y.X. performed the experiments and R.O. supervised the project. Y.X. and R.O. wrote the manuscript.

## Competing interests

The authors declare no competing interests.

## Additional information

**Extended data** is available for this paper at <https://doi.org/10.1038/s41477-020-0650-2>.

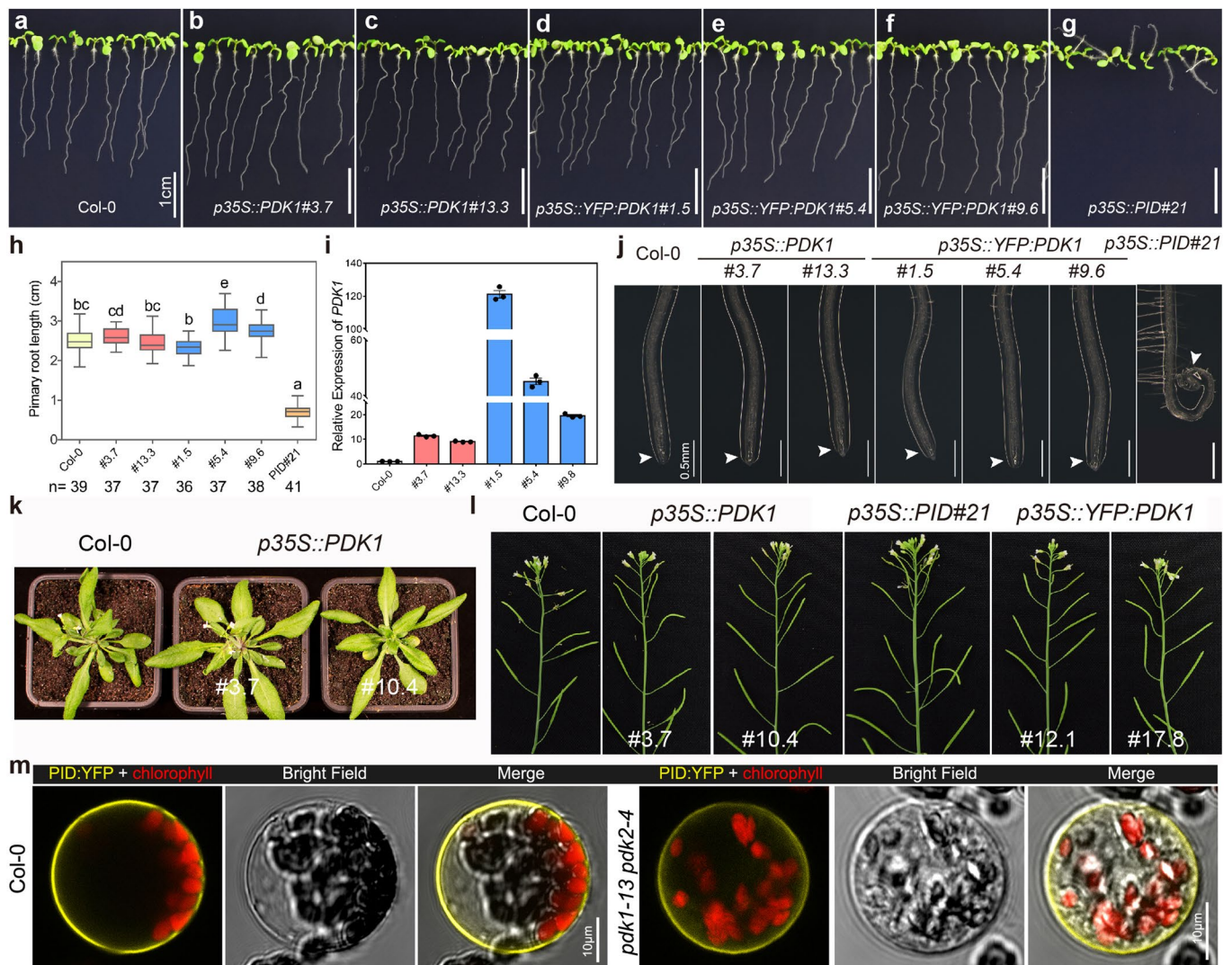
**Supplementary information** is available for this paper at <https://doi.org/10.1038/s41477-020-0650-2>.

**Correspondence and requests for materials** should be addressed to u.-s.a.O.

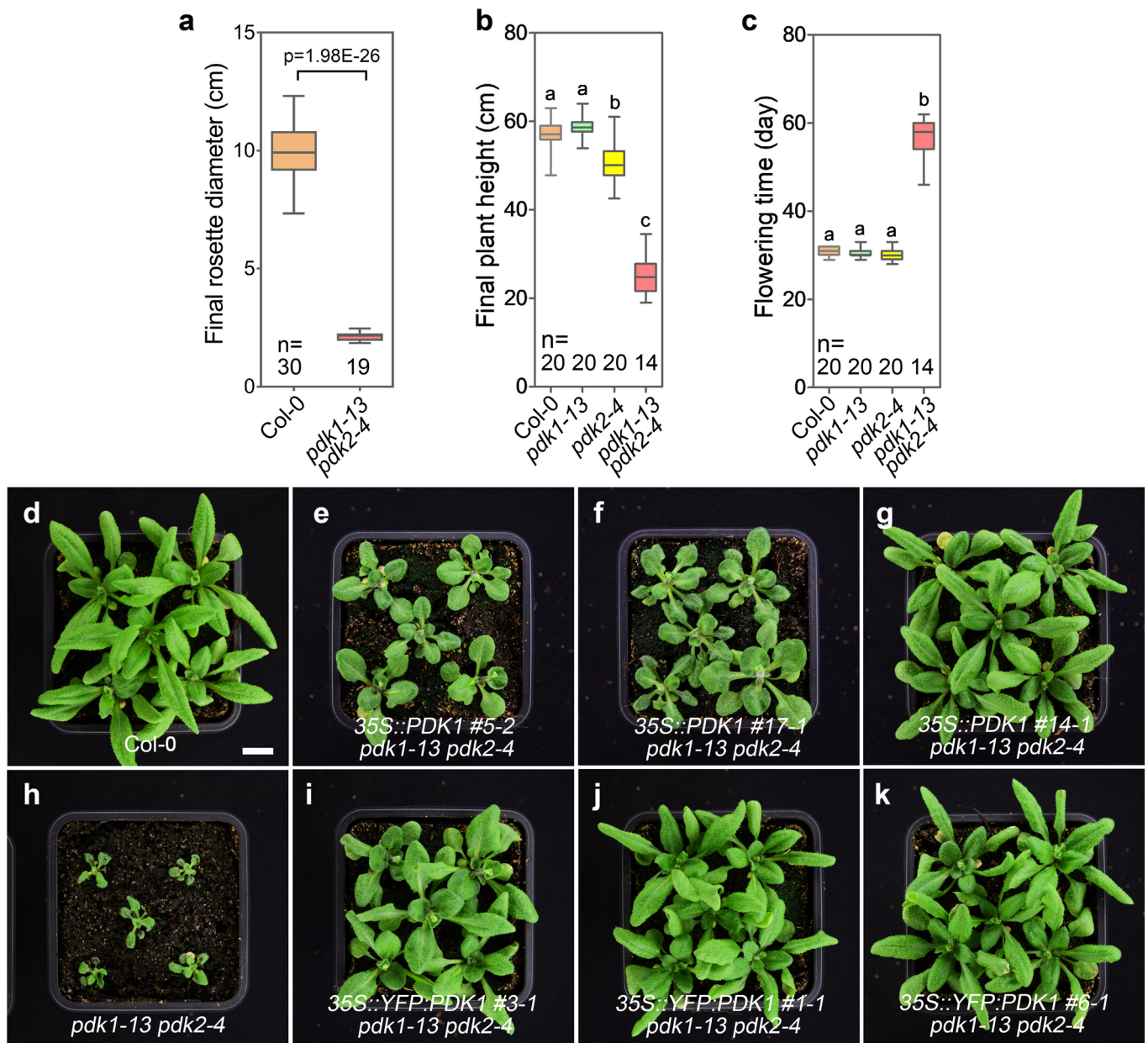
**Reprints and permissions information** is available at [www.nature.com/reprints](http://www.nature.com/reprints).

**Publisher's note** Springer Nature remains neutral with regard to jurisdictional claims in published maps and institutional affiliations.

© The Author(s), under exclusive licence to Springer Nature Limited 2020

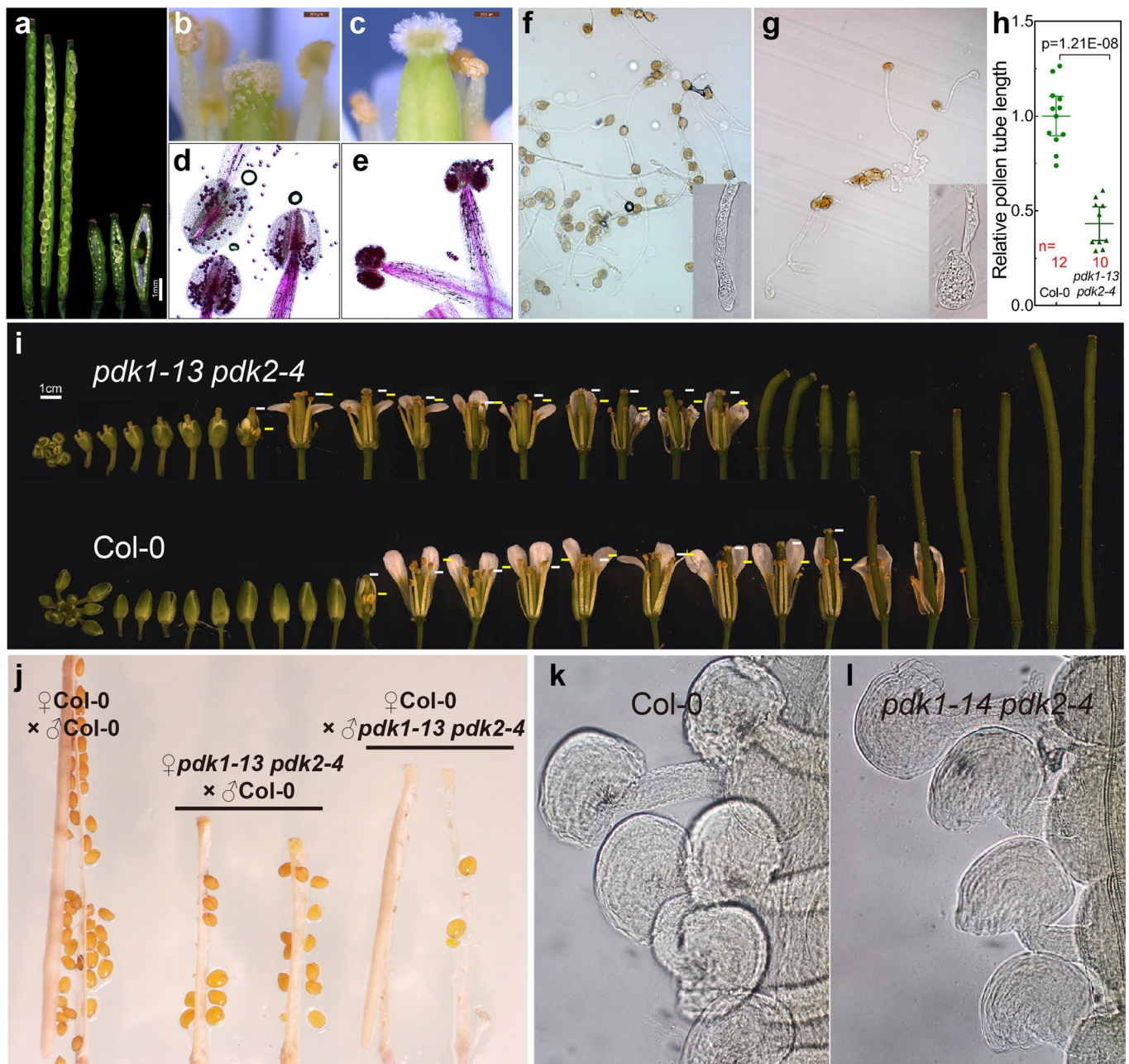


**Extended Data Fig. 1 | Relevance of PDK1 for PID function in planta.** **a–g**, Representative 7-day-old seedlings of the indicated lines. Please note that only *p35S::PID#21* seedlings show agravitropic growth. Scale bars represent 1 cm. Similar results have been obtained in four independent experiments. **h**, Box plot showing the quantification of the primary root length of 7-day-old seedlings of *Arabidopsis* wild type (Col-0), *p35S::PDK1* lines #3.7 and 13.3 (red box), *p35S::YFP:PDK1* lines #1.5, 5.4 and 9.6 (blue box), and *p35S::PID* line #21. *n* indicates the number of measured roots, the results are from a single experiment, but similar results were obtained in three independent experiments. Lower case letters indicate statistically different groups ( $p < 0.05$ , details of statistical analysis are provided in Supplementary Table 4), as determined by a one-way ANOVA followed by Tukey's test. Boxes indicate 1<sup>st</sup> and 3<sup>rd</sup> quartile, the horizontal line in a box the median, whiskers the maximum and minimum. **i**, PDK1 expression levels in Col-0 and in the *p35S::PDK1* and *p35S::YFP:PDK1* lines used in **h**. The bar graph shows the mean value  $\pm$  SEM ( $n = 3$  technical repeats). **j**, Representative images showing a detail of the root tip phenotype of seedlings in **a–h**. White arrow heads point out collapsed (*p35S::PID#21*) or normal root meristems (all other lines;  $n = 40$  independent seedling roots were checked for each line). Scale bars indicate 0.5 mm. **k**, One-month-old Col-0 and *PDK1* overexpression plants ( $n = 10$  independent plants were observed per line). **l**, Inflorescence phenotype of Col-0, *PID*- and *PDK1* overexpression lines ( $n = 12$  independent plants were observed per line). **m**, Representative images of *PID:YFP* subcellular localization in Col-0 or *pdk1-13 pdk2-4* protoplasts. Eleven wild-type (Col-0) and fourteen *pdk1-3 pdk2-4* mutant protoplasts were observed in this experiment, and all showed the similar localization. For **h–m**, Three biological repeats showed similar results.

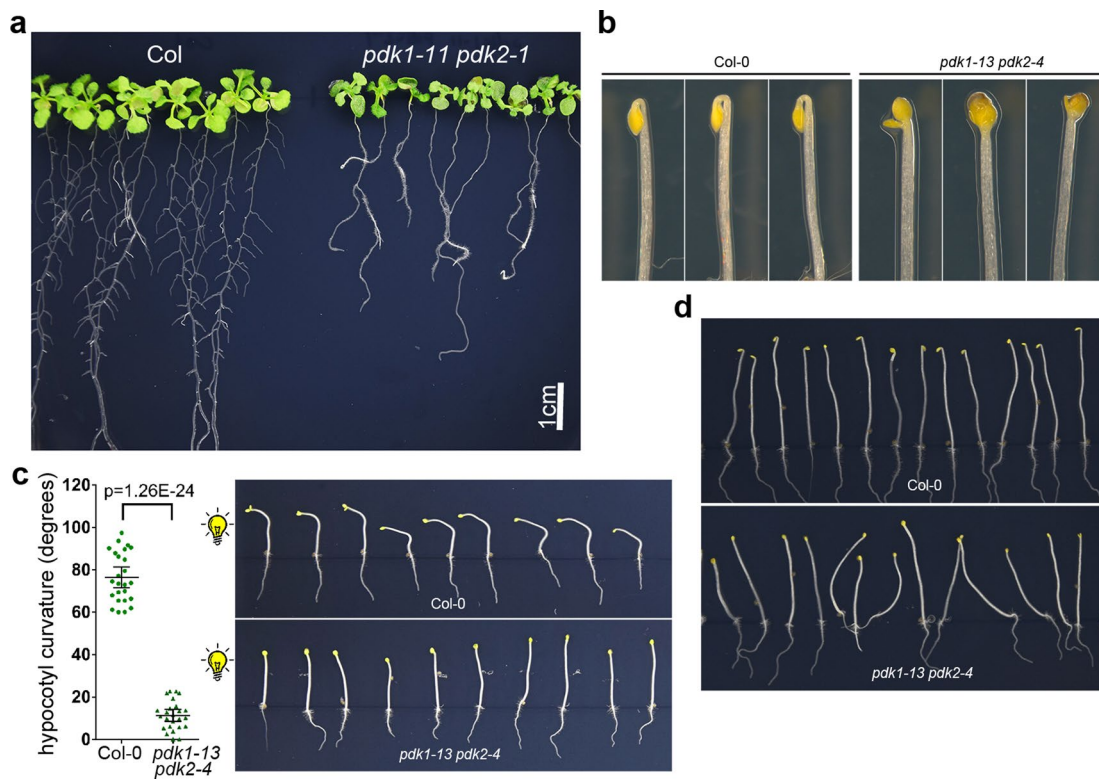


**Extended Data Fig. 2 | Quantification of *pdk1 pdk2* mutant phenotypes and complementation of the mutant by *35S::PDK1* or *35S::YFP:PDK1*.**

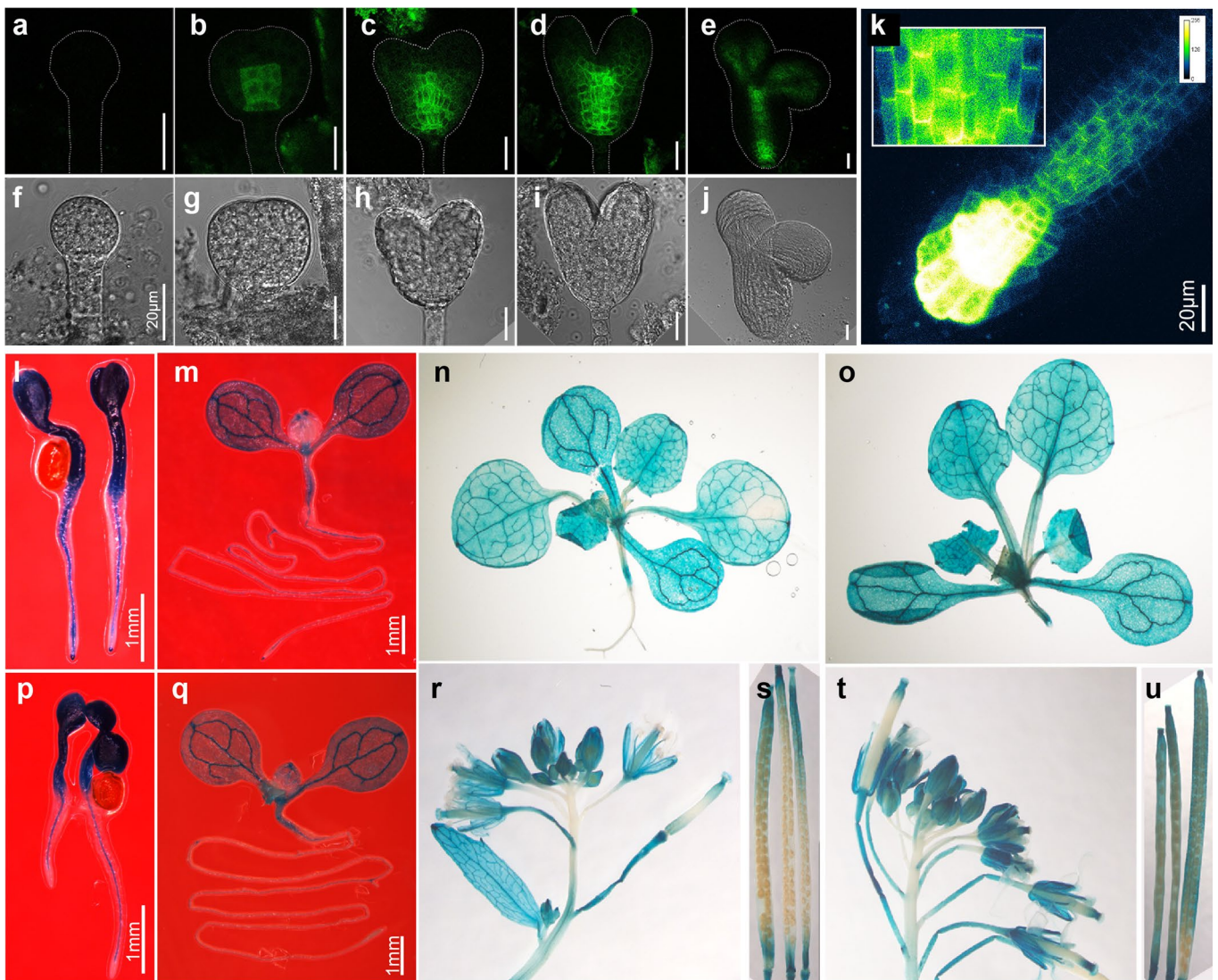
**a**, Quantification of the rosette diameter of 30-day-old *Arabidopsis* wild-type (Col-0) and *pdk1-13 pdk2-4* plants. A two-sided Student *t*-test was used for statistical analysis. **b**, Final heights of the indicated plant lines. **c**, Flowering time of the indicated lines. Lower case letters in **b** and **c** indicate statistical differences, as determined by one-way analysis of variance (ANOVA) followed by Tukey's test ( $p < 0.05$ , details of statistical analysis are provided in Supplementary Table 4). *n* indicates the number of independent plants used for measurements in **a-c**. Boxes indicate 1<sup>st</sup> and 3<sup>rd</sup> quartile, the horizontal line in a box the median, whiskers the maximum and minimum. **d-k**, Plants of wild-type (Col-0), *pdk1-13 pdk2-4* and representative complementation lines were grown on plates for 10 days and subsequently in soil for 20 days before photographing. 15 plants were observed in a single experiment for each line. For **a-k**, three independent experiments showed similar results.



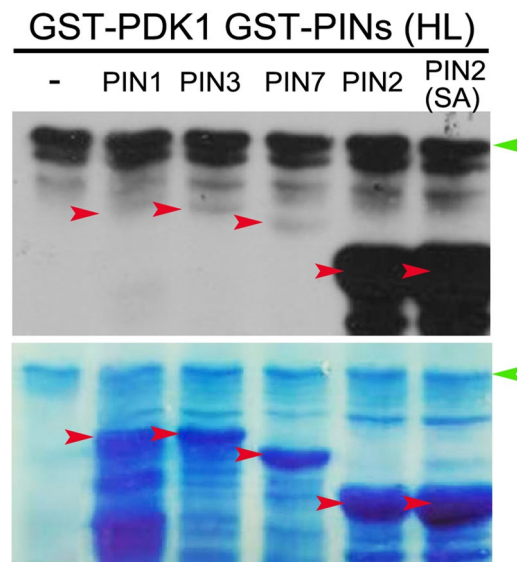
**Extended Data Fig. 3 | *pdk1 pdk2* mutant phenotypes in reproductive tissues.** **a**, *pdk1 pdk2* siliques (three on the right) are much shorter than wild-type siliques (three on the left), and contain many unfertilized ovules. **b** and **c**, Difference in pollen grain deposition on the stigma of a wild-type (**b**) or a *pdk1-13 pdk2-4* mutant (**c**) flower. **d** and **e**, Mature wild-type (**d**) or *pdk1-13 pdk2-4* mutant (**e**) anthers stained with Alexander's showing that pollen grains are viable, but that mutant anthers do not sufficiently dehisce. **f** and **g**, *In vitro* germination of wild-type (**f**) and *pdk1-13 pdk2-4* mutant (**g**) pollen. A detail of pollen tube tip is shown in the inset. **h**, Relative pollen tube length after 18 hours incubation. The average length of wild-type (Col-0) pollen tubes is put at 1.0. A two sided Student's *t*-test was used for statistical analysis, *n* indicates the number of independent pollen tubes measured. Means with 95% confidence intervals are shown. **i**, Developmental series of *pdk1-13 pdk2-4* mutant and wild-type (Col-0) flowers. The white bars indicate the position of the gynoecium apex, the yellow bars indicate the position of the anthers. **j**, Ripe siliques with the valves removed, derived from reciprocal crosses between wild-type *Arabidopsis* (Col-0) and the *pdk1-13 pdk2-4* loss-of-function mutant. **k** and **l**, Representative DIC images showing the phenotype of wild-type (Col-0) (**k**, *n* = 330) or *pdk1-14 pdk2-4* mutant (**l**, *n* = 306) ovules. For **a-l**, similar results were obtained in three independent experiments.



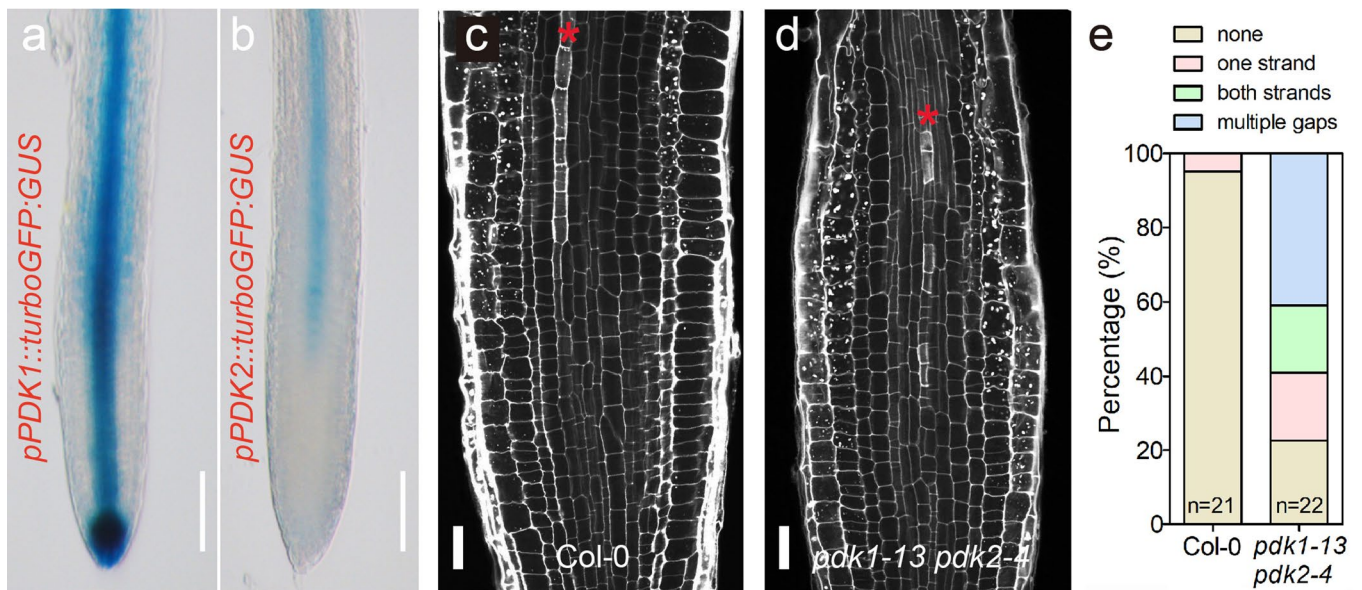
**Extended Data Fig. 4 | *pdk1 pdk2* mutant seedlings phenocopy *d6pk012* triple mutants.** **a**, Phenotype of 15-day-old wild-type (Col-0) and *pdk1-11 pdk2-1* seedlings grown on vertical plates. **b**, Apical hook phenotype of 4-day-old wild-type (Col-0) and *pdk1-13 pdk2-4* etiolated seedlings. **c**, Hypocotyl curvature after 18 h directional white light treatment on 4-day-old etiolated wild-type (Col-0) and *pdk1-13 pdk2-4* seedlings ( $n = 25$  independent seedlings). A two sided Student's *t*-test was used for statistical analysis. Means with 95% confidence intervals are shown. **d**, 5-day-old wild-type (Col-0) and *pdk1-13 pdk2-4* seedlings grown in dark. Note the agravitropic hypocotyl growth of *pdk1-13 pdk2-4* mutant seedlings. For **a** and **d**, five independent experiments showed similar results. For **b** and **c**, three independent experiments showed similar results.



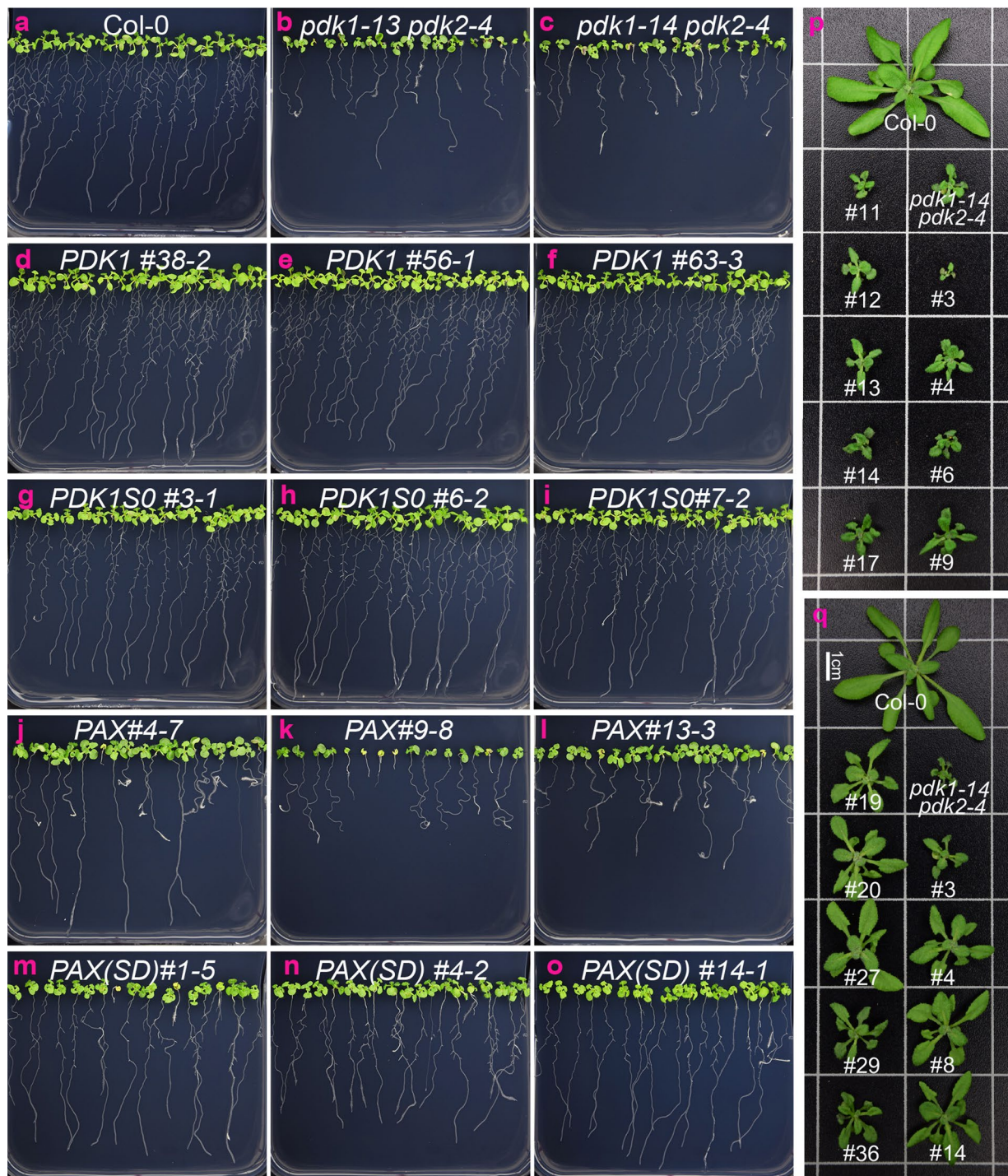
**Extended Data Fig. 5 | *PDK1* and *PDK2* are predominantly expressed in (pro) vascular tissues, where *PDK1* associates with the basal PM.** **a–j**, *PDK1* expression is confined to the provascular tissue during *Arabidopsis* embryo development. Confocal (**a–e**), and bright field images (**f–j**) of *Arabidopsis* *pPDK1::YFP::PDK1* 16-cell (**a, f**), globular (**b, g**), heart (**c, h**), late heart (**d, i**), and torpedo (**e, j**) stage embryos. **k**, Confocal images of a 4-day-old *pPDK1::YFP::PDK1* root tip. The inset shows a detail of YFP::PDK1 localization in root stele cells. **l–u**, Spatio-temporal expression pattern of *PDK1* (**l, m, n, r, s**) and *PDK2* (**p, q, o, t, u**) as reported by histochemical staining of 3-day-old seedlings (**l, p**), 7-day-old seedlings (**m, q**), 16-day-old plants (**n, o**) and inflorescences and siliques from 40-day-old plants (**r–u**) of representative *pPDK1-GG* and *pPDK2-GG* lines, respectively. Similar results were obtained with three independent lines in three biological repeats.



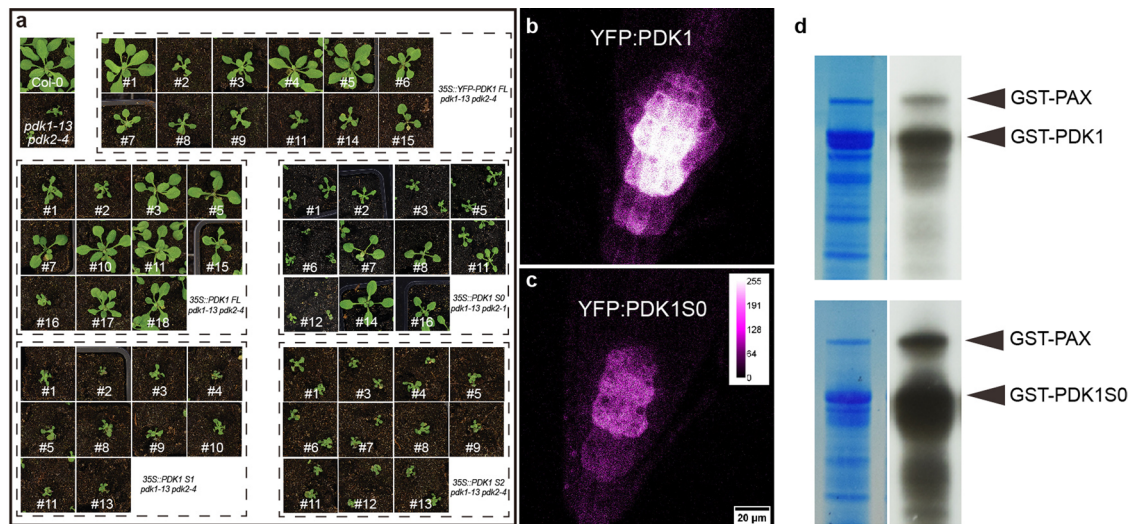
**Extended Data Fig. 6 | PDK1 strongly phosphorylates the PIN2 central hydrophilic loop (PIN2HL) in a S1, S2, S3-independent manner *in vitro*.** Only very weak (probably non-specific) phosphorylation is observed for the PIN1HL, PIN3HL or PIN7HL. Red or green arrows point out the position of the GST-PINHL or GST-PDK1, respectively. Upper: autoradiograph, lower: PageBlue stained gel. Similar results were obtained in three independent experiments.



**Extended Data Fig. 7 | PDK1 and PDK2 are expressed in primary root vascular tissue to control phloem differentiation.** **a, b**, DIC microscopy images of roots of 5-day-old *PDK1* (**a**) and *PDK2* (**b**) promoter::turboGFP-GUS seedlings stained for GUS activity. Bar = 0.1 mm. **c, d**, Confocal sections of mPS-PI stained wild-type (Col-0, **c**) and *pdk1-13 pdk2-4* (**d**) roots. The protophloem cell layer is indicated with a red asterisk. Bar = 10  $\mu$ m. **e**, Quantification of gaps in PPSEs in wild-type and *pdk1-13 pdk2-4* roots. The number of observed roots (n) is indicated in each bar. Three biological repeats showed similar results.

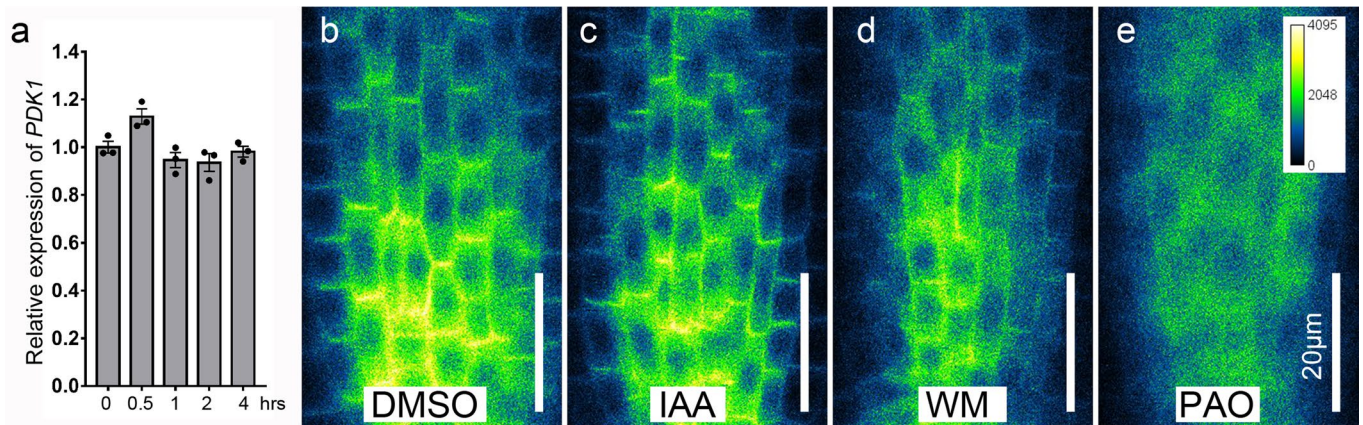


**Extended Data Fig. 8 | Complementation of the *pdk1 pdk2* mutant by *PDK1* promoter driven YFP:PDK1, YFP:PDK1S0 or YFP:PAX(SD) expression.** **a-o**, Phenotype of 13-day-old seedlings of the indicated lines grown on vertical plates. *pdk1 pdk2 pPDK1::YFP* is omitted in (d-o) for presentation purposes. **j-l**, Note that YFP:PAX only shows partial complementation in the high expressing line #4.7 (see also Fig. 4a). Five biological repeats showed similar results. **p and q**, *pPDK1::YFP:PAX (SD)* partially rescues the dwarf rosette phenotype of *pdk1-14 pdk2-4* (q), whereas *pPDK1::YFP:PAX* does not (p). Rosette phenotype of 26-day-old wild-type (Col-0), *pdk1-14 pdk2-4* mutant, or *pPDK1::YFP:PAX pdk1-14 pdk2-4* (p) or *pPDK1::YFP:PAX(SD) pdk1-14 pdk2-4* (q) plants. For the latter two, representative plants of nine independent lines are shown. Similar results were obtained in the T2, T3 and T4 generation.



**Extended Data Fig. 9 | PDK1 promoter-driven expression of the cytosolic PDK1S0 isoform rescues the *pdk1 pdk2* mutant rosette phenotype.**

**a**, Complementation assay for overexpression of cDNAs representing the different *PDK1* splice variants in the *pdk1 pdk2* mutant background. Plants were grown on plates for 10 days, and subsequently transferred to and grown in soil for 10 days. Similar results were obtained in the T2, T3 and T4 generation. **b** and **c**, Subcellular localization of *PDK1* promoter driven YFP:PDK1 (**b**, the line with lowest expression level obtained) and YFP:PDK1S0 (**c**, the line with highest expression level obtained) in root columella cells. Ten roots were observed per independent experiment for each line. **d**, PDK1S0 (lower panel) has a higher auto- and trans-phosphorylation activity compared to PDK1 (upper panel). Coomassie stained gel (left) and autoradiograph (right) are shown, and positions of the GST-tagged PAX, -PDK1 and -PDK1S0 are indicated. For **b-d**, similar results have been obtained in three independent experiments.



**Extended Data Fig. 10 | *PDK1* expression and YFP:PDK1 subcellular localization after chemical treatment.** **a**, Relative *PDK1* transcript levels are not significantly changed in 5-day-old seedlings following 0.5 to 4 hours treatment with 1 µM indole-3-acetic acid (IAA). Bars with error bars indicate mean ± SEM (n=3 technical repeats). **b-e**, Confocal images of *pdk1 pdk2 pPDK1::YFP:PDK1* roots showing YFP:PDK1 localization after 1 hour treatment with DMSO (**b**), 1 µM IAA (**c**) or 33 µM wortmannin (WM) (**d**), or 30 min treatment with 30 µM phenylarsine oxide (PAO) (**e**). For **a-e**, Similar results have been obtained in three biological repeats.

## Reporting Summary

Nature Research wishes to improve the reproducibility of the work that we publish. This form provides structure for consistency and transparency in reporting. For further information on Nature Research policies, see [Authors & Referees](#) and the [Editorial Policy Checklist](#).

### Statistics

For all statistical analyses, confirm that the following items are present in the figure legend, table legend, main text, or Methods section.

n/a Confirmed

- The exact sample size ( $n$ ) for each experimental group/condition, given as a discrete number and unit of measurement
- A statement on whether measurements were taken from distinct samples or whether the same sample was measured repeatedly
- The statistical test(s) used AND whether they are one- or two-sided  
*Only common tests should be described solely by name; describe more complex techniques in the Methods section.*
- A description of all covariates tested
- A description of any assumptions or corrections, such as tests of normality and adjustment for multiple comparisons
- A full description of the statistical parameters including central tendency (e.g. means) or other basic estimates (e.g. regression coefficient) AND variation (e.g. standard deviation) or associated estimates of uncertainty (e.g. confidence intervals)
- For null hypothesis testing, the test statistic (e.g.  $F$ ,  $t$ ,  $r$ ) with confidence intervals, effect sizes, degrees of freedom and  $P$  value noted  
*Give  $P$  values as exact values whenever suitable.*
- For Bayesian analysis, information on the choice of priors and Markov chain Monte Carlo settings
- For hierarchical and complex designs, identification of the appropriate level for tests and full reporting of outcomes
- Estimates of effect sizes (e.g. Cohen's  $d$ , Pearson's  $r$ ), indicating how they were calculated

*Our web collection on [statistics for biologists](#) contains articles on many of the points above.*

### Software and code

Policy information about [availability of computer code](#)

Data collection

n.a.

Data analysis

Image J (Fiji), GraphPad Prism 5, ClustalW in MEGA-X, InterPro online tool

For manuscripts utilizing custom algorithms or software that are central to the research but not yet described in published literature, software must be made available to editors/reviewers. We strongly encourage code deposition in a community repository (e.g. GitHub). See the Nature Research [guidelines for submitting code & software](#) for further information.

### Data

Policy information about [availability of data](#)

All manuscripts must include a [data availability statement](#). This statement should provide the following information, where applicable:

- Accession codes, unique identifiers, or web links for publicly available datasets
- A list of figures that have associated raw data
- A description of any restrictions on data availability

A data availability statement has been included in the manuscript

## Field-specific reporting

Please select the one below that is the best fit for your research. If you are not sure, read the appropriate sections before making your selection.

- Life sciences       Behavioural & social sciences       Ecological, evolutionary & environmental sciences

For a reference copy of the document with all sections, see [nature.com/documents/nr-reporting-summary-flat.pdf](https://www.nature.com/documents/nr-reporting-summary-flat.pdf)

## Life sciences study design

All studies must disclose on these points even when the disclosure is negative.

Sample size	Sample size was chosen based on what is commonly used in the field
Data exclusions	No data were excluded
Replication	The number of experimental replications is indicated in the figure legends.
Randomization	Seedlings and plants with the same genetic background were picked randomly for data collecting.
Blinding	Blinding is not relevant for our study, since different genetic background alleles have obviously different phenotypes.

## Reporting for specific materials, systems and methods

We require information from authors about some types of materials, experimental systems and methods used in many studies. Here, indicate whether each material, system or method listed is relevant to your study. If you are not sure if a list item applies to your research, read the appropriate section before selecting a response.

### Materials & experimental systems

n/a	Involvement in the study
<input checked="" type="checkbox"/>	<input type="checkbox"/> Antibodies
<input checked="" type="checkbox"/>	<input type="checkbox"/> Eukaryotic cell lines
<input checked="" type="checkbox"/>	<input type="checkbox"/> Palaeontology
<input checked="" type="checkbox"/>	<input type="checkbox"/> Animals and other organisms
<input checked="" type="checkbox"/>	<input type="checkbox"/> Human research participants
<input checked="" type="checkbox"/>	<input type="checkbox"/> Clinical data

### Methods

n/a	Involvement in the study
<input checked="" type="checkbox"/>	<input type="checkbox"/> ChIP-seq
<input checked="" type="checkbox"/>	<input type="checkbox"/> Flow cytometry
<input checked="" type="checkbox"/>	<input type="checkbox"/> MRI-based neuroimaging